Calorimetry – part 2

Riccardo Paramatti

INFN Roma

Joint Belgian Dutch German Graduate School

Kerkrade – 4th September 2014

Outline

- The electromagnetic and hadronic calorimeters of ATLAS and CMS experiments will be described in all the relevant aspects:
  - design choice
  - construction
  - commissioning
  - calibration
  - stability
  - performance during LHC Run1

Caveat: more details on the CMS ECAL since it is the only homogeneous calorimeter among ATLAS and CMS

Physics requirements for calorimeters at LHC

- High resolution and high granularity electromagnetic calorimeter:
  - to detect the two photon decay of an intermediate mass Higgs (golden channel together with $H \to ZZ$)
  - very precise measurements of Standard Model *candles* as $Z \to ee$ and $W \to e\nu$
- Hermetic hadron calorimeter:
  - coverage up to $|\eta| \sim 5$ to tag very forward jets and good measurement of the missing transverse energy (light SUSY particles).

Experimental conditions at LHC

Machine luminosity $\rightarrow 10^{34}\ \mathrm{cm^{-2}\,s^{-1}}$
$\sigma_{inel} \sim 100$ mb $\rightarrow 10^{9}$ events/s
$\sigma_{higgs} \sim 1$ pb $\rightarrow 10^{-2}$ events/s

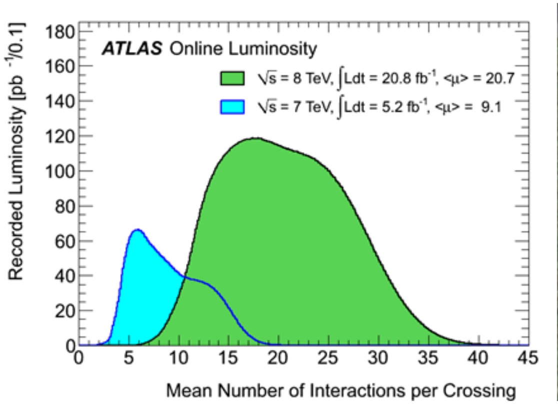

20 events/crossing $\rightarrow$1000 tracks
1 bunch crossing every 25ns

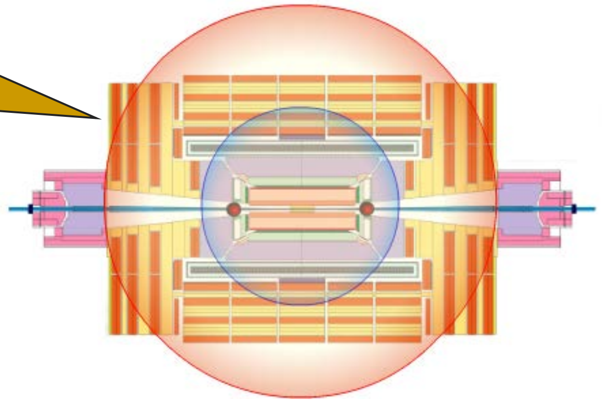

Extreme conditions for detectors

- Granularity ($10^5 \div 10^7$ channels)
- Speed of response
- DAQ + trigger ($10^9 \rightarrow \sim 5\text{x}10^2$ ev/s)
- High radiation resistance

An introduction to CMS calorimeters

Crystal choice for CMS electromagnetic calorimeter

	NaI(Tl)	BaF_2	CsI(Tl)	CsI	CeF_3	BGO	PWO	
ρ	3.67	4.88	4.53	4.53	6.16	7.13	8.26	g/cm^3
X0	2.59	2.05	1.85	1.85	1.68	1.12	0.89	cm
RM	4.5	3.4	3.8	3.8	2.6	2.4	2.2	cm
τ	250	0.8/620	1000	20	30	300	15	ns
λp	410	220/310	565	310	310/340	480	420	nm
n (λp)	1.85	1.56	1.80	1.80	1.68	2.15	2.29	
LY	100%	15%	85%	7%	5%	10%	0.2%	%NaI

Typical light yield of NaI ~ 40000 γ/MeV

CMS ECAL: the choice of $PbWO_4$

☺

- Fast scintillation
- Small X_0 and R_m
- Radiation hardness
- Relatively easy to grow

☹ → will see how to face the cons

- Low Light Yield
- High index of refraction
- Strong LY dependence on T

Parameter		Value
Radiation length	cm	0.89
Moliere radius	cm	2.2
Hardness	Moh	4
Refractive index		2.3
Peak emission	nm	440
% of light in 25 ns		80%
Light yield (23 cm)	γ/MeV	100

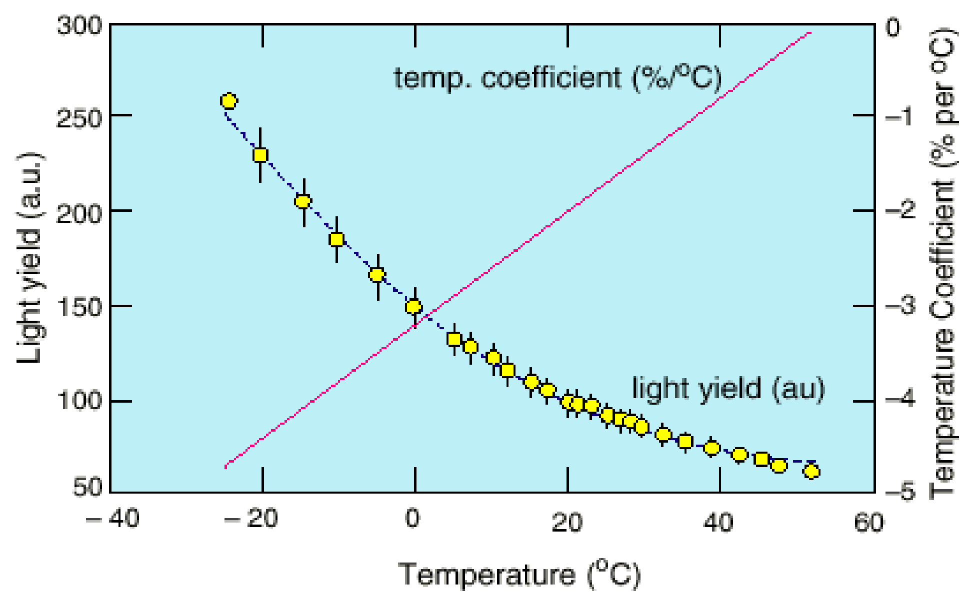

From ingots to crystals

- Crystal R&D phase (1995-1998)
- 6000 crystal preproduction (1998-2000)
- Crystal production:
  2001-2006 Barrel
  2006-2007 Endcap

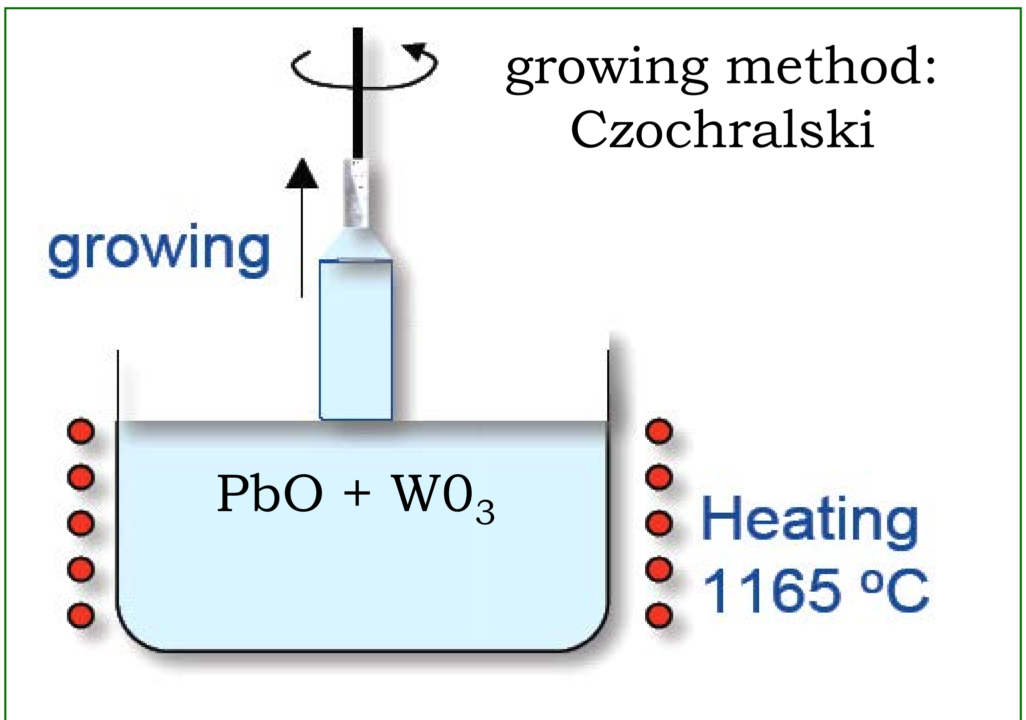

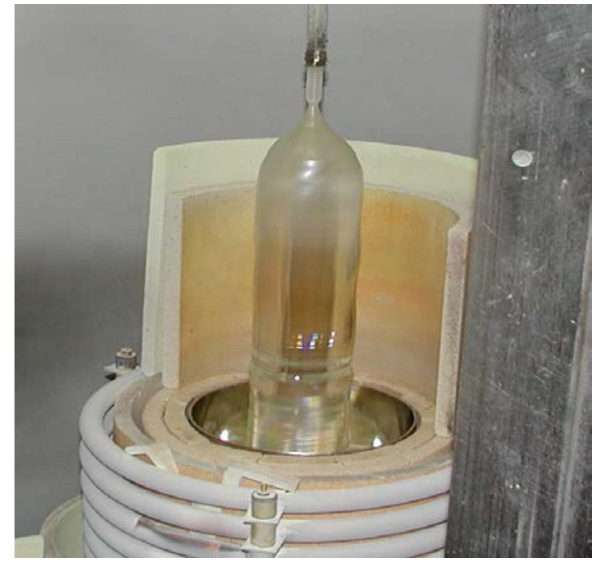

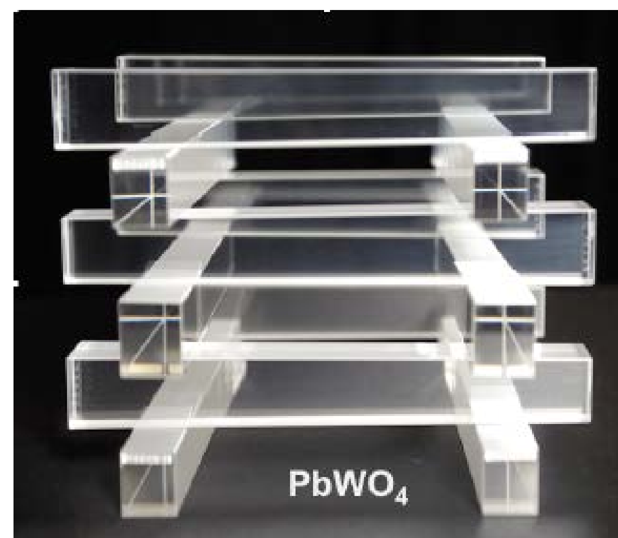

Crystal + photodetector

- Incident electron/photon generates EM shower (spread laterally over several crystals) in the heavy $PbWO_4$ material
  - Charged particles in the shower produce scintillation light isotropically
  - Amount of scintillation light is proportional to incident particle energy
  - Scintillation light detected by photodetectors with internal amplification:
    Silicon Avalanche PhotoDiodes - APDs (in EB)
    Vacuum PhotoTriodes - VPTs (in EE)

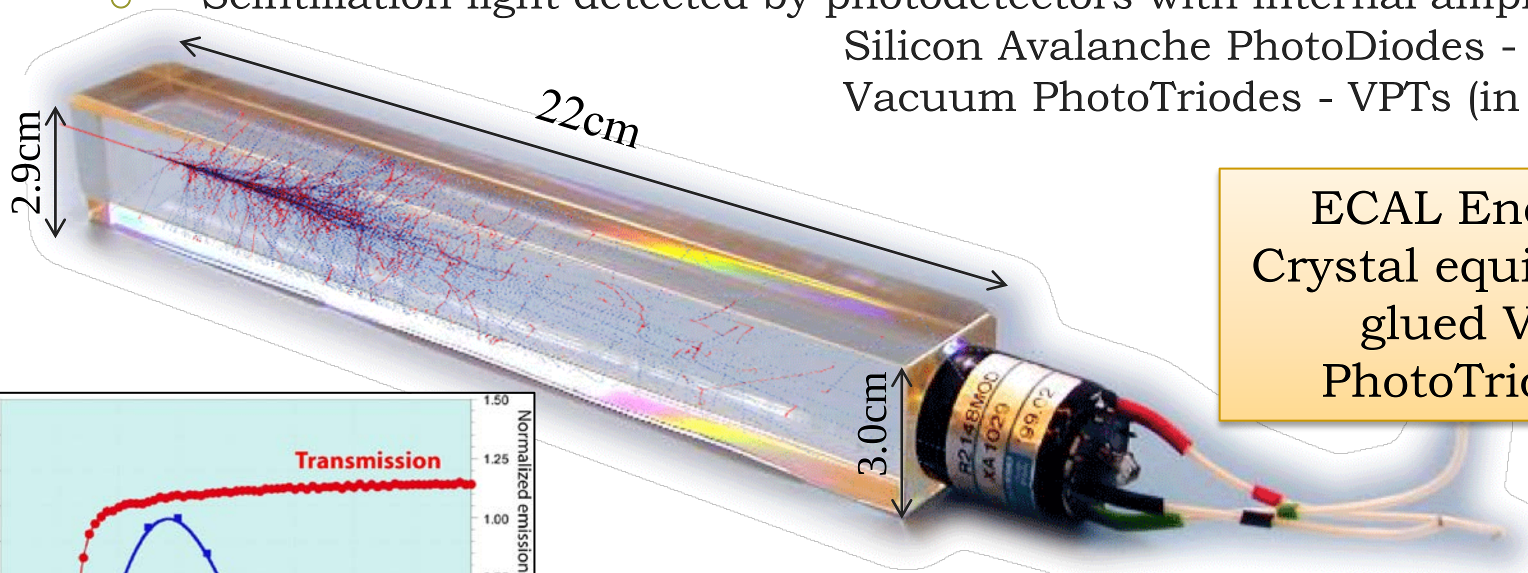

ECAL Endcap (EE) Crystal equipped with a glued Vacuum PhotoTriode (VPT)

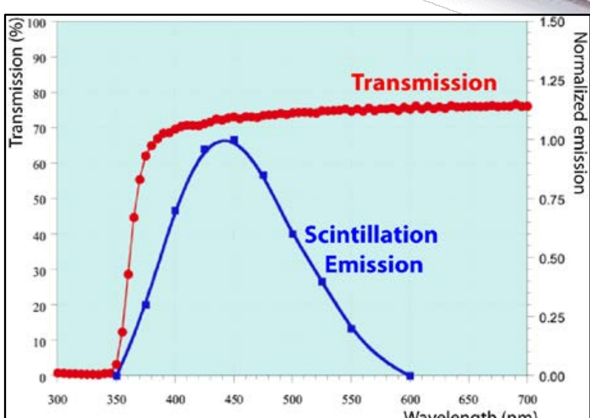

$PbWO_4$ crystals are transparent to the entire scintillation emission spectrum – before irradiation (see part 3)

Photo-detector devices

- Scintillating crystals and Cerenkov quartz fibers produce light proportional to the energy lost by incoming particle
- Light converted to analog signal with photo-detector
- Design constraints:
  - Quantum efficiency (probability to convert an incoming photon into a photoelectron) meshes with light output
  - Internal gain (fundamental for low light yield detectors)
  - Environment – magnetic field, radiation
  - Readout requirements – single or multi-anode photo-multiplier
  - Sensitive to wavelength of light from active detector (or WaveLength Shifter to collect light)

CMS ECAL photo-detectors

- Most common photo-detectors not suitable:
  - Photomultipliers (because affected by magnetic field and too large volume)
  - PIN photodiodes (because no internal amplification and too sensitive to charged particles)

Barrel - Avalanche photodiodes (APD)

Two 5x5 mm^2 APDs/crystal, ~ 4.5pe/MeV
- Gain: 50   QE: ~75% @ λ_{peak}= 420 nm
- Gain dependence on T & V: $\Delta G/\Delta T$ = -2.4%/°C, $\Delta G/\Delta V$ = 3.1%/V
- Excess noise factor F=2.2 (fluctuation in multiplication)
- *Some sensitivity to direct ionization*

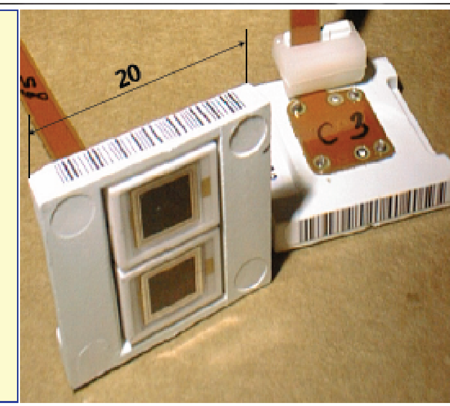

Endcaps: - Vacuum phototriodes (VPT)
- Active area ~ 280 mm^2/crystal ~4.5pe/MeV
- Gain 8 -10 (B=4T)   Q.E.~20% at 420 nm
- *Aeging with cumulated charge*

APD excess noise factor

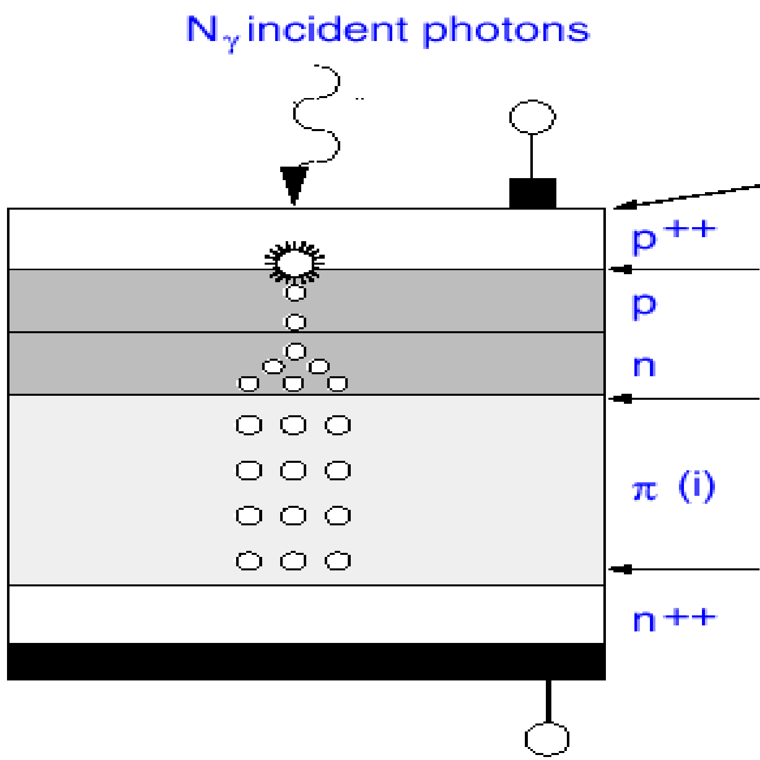

quantum efficiency: ε_Q

$N_{pe} = N_\gamma \, \varepsilon_Q$

stochastic process: $N_{pe} \pm \sqrt{N_{pe}}$

gain $M \pm \sigma_M$

$N_e = M \times N_{pe}$

photoelectron statistics

$M \times N_{pe} \pm M \sqrt{N_{pe}}$

multiplication fluctuations

$M \times N_{pe} \pm \sigma_M \sqrt{N_{pe}}$

$$\frac{\sigma_{Ne}}{N} = \frac{1}{\sqrt{N_{pe}}} \frac{\sqrt{M^2 + \sigma_M^2}}{M} = \sqrt{\frac{F}{N_{pe}}}$$

CMS Electromagnetic Calorimeter

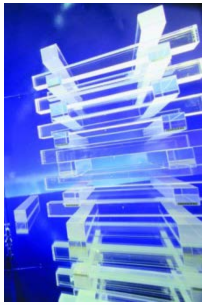

- Lead Tungstate ($PbWO_4$) homogenous crystal calorimeter
- Barrel (EB):
  - 36 Supermodules (SM), each 1700 crystals
  - $|\eta|<1.48$
  - APD photodetectors
- Endcaps (EE):
  - 2 Endcap sides, each 7324 crystals
  - $1.48<|\eta|<3.0$
  - VPT photodetectors
- Preshower (ES):
  - sampling calorimeter (lead, silicon strips)
  - $1.65<|\eta|<2.6$

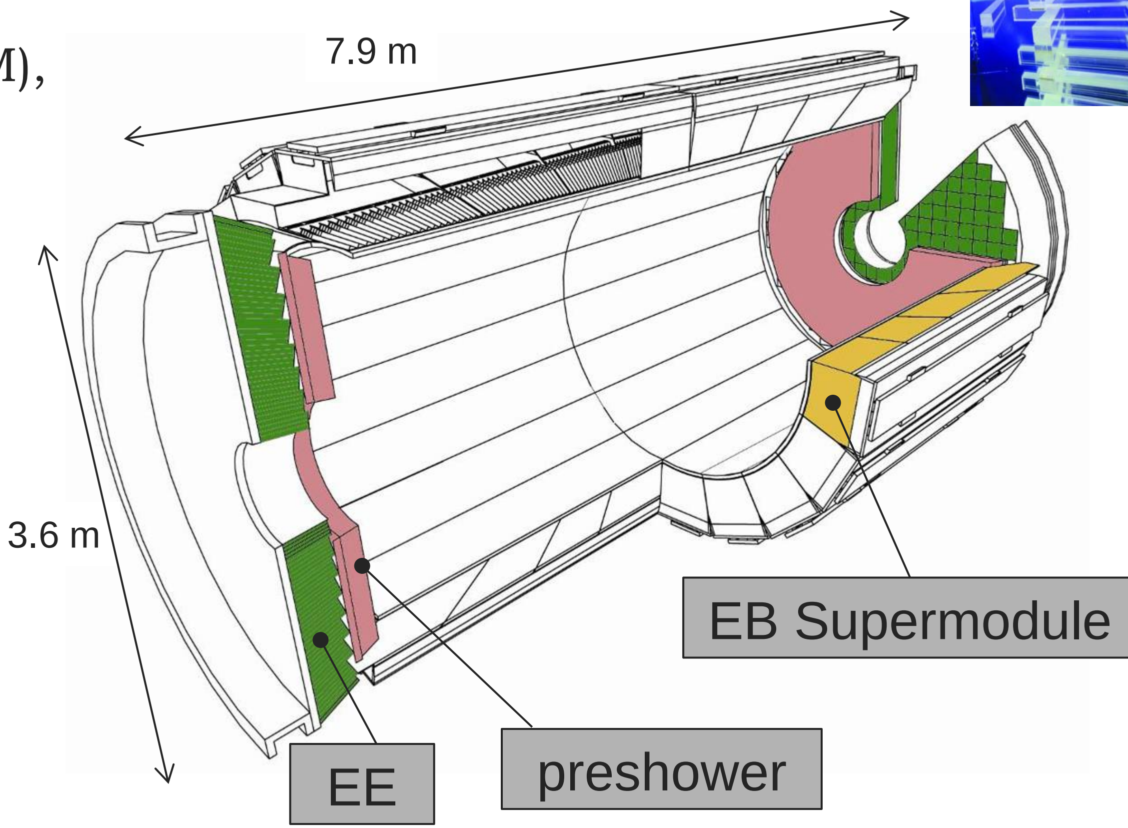

The calorimeter preshower

One of the main physics goals of CMS is search for SM Higgs

If m_H < 150 GeV/c^2 the golden channel is through diphoton decay

But large reducible background from π^0 faking single photons

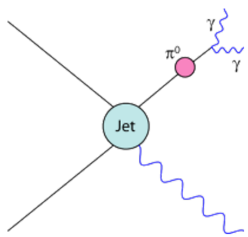

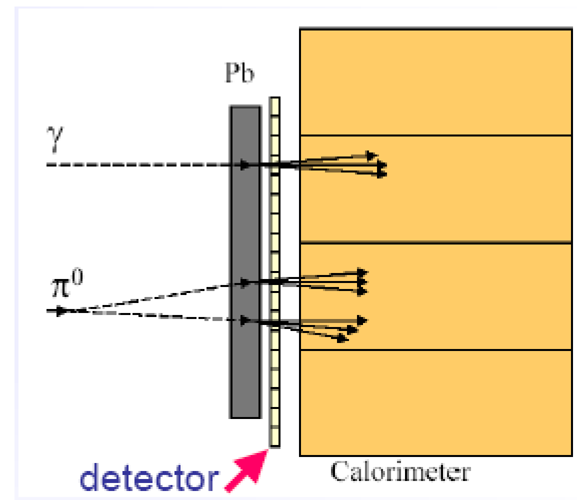

- Photon and π^0 although very similar in the calorimeter have different topology in the preshower.

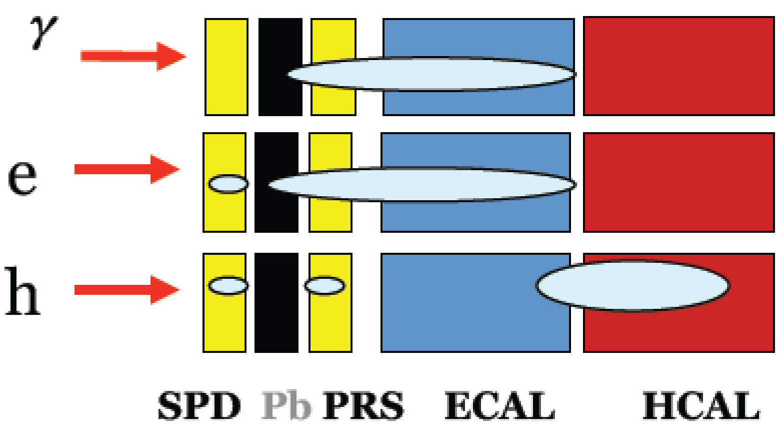

- Preshower also used in LHCb to separate photon, electron and hadron at the trigger level

CMS Hadronic Calorimeter

- Requirements:
  - hermetic and compact
  - radiation tolerant
  - reasonable energy resolution
- Sampling calorimeter with longitudinal segmentation
- Hadronic Barrel and Endcap calorimeters:
  - sampling brass/plastic scintillator tiles
  - additional scintillator layer outside the solenoid cryostat
- The forward calorimeter:
  - steel absorber and Cerenkov-producing quartz fiber
  - outside the solenoid cryostat
  - coverage up to $|\eta|<5.2$

CMS Hadronic Barrel and Endcap sampling calorimeter

- Incident charged/neutral hadron generates shower in the heavy brass absorber
  - Charged particles in the shower produce scintillation light in the plastic
  - Amount of scintillation light is proportional to incident particle energy
  - Light shifted in wavelength and transported to Hybrid PhotoDiodes

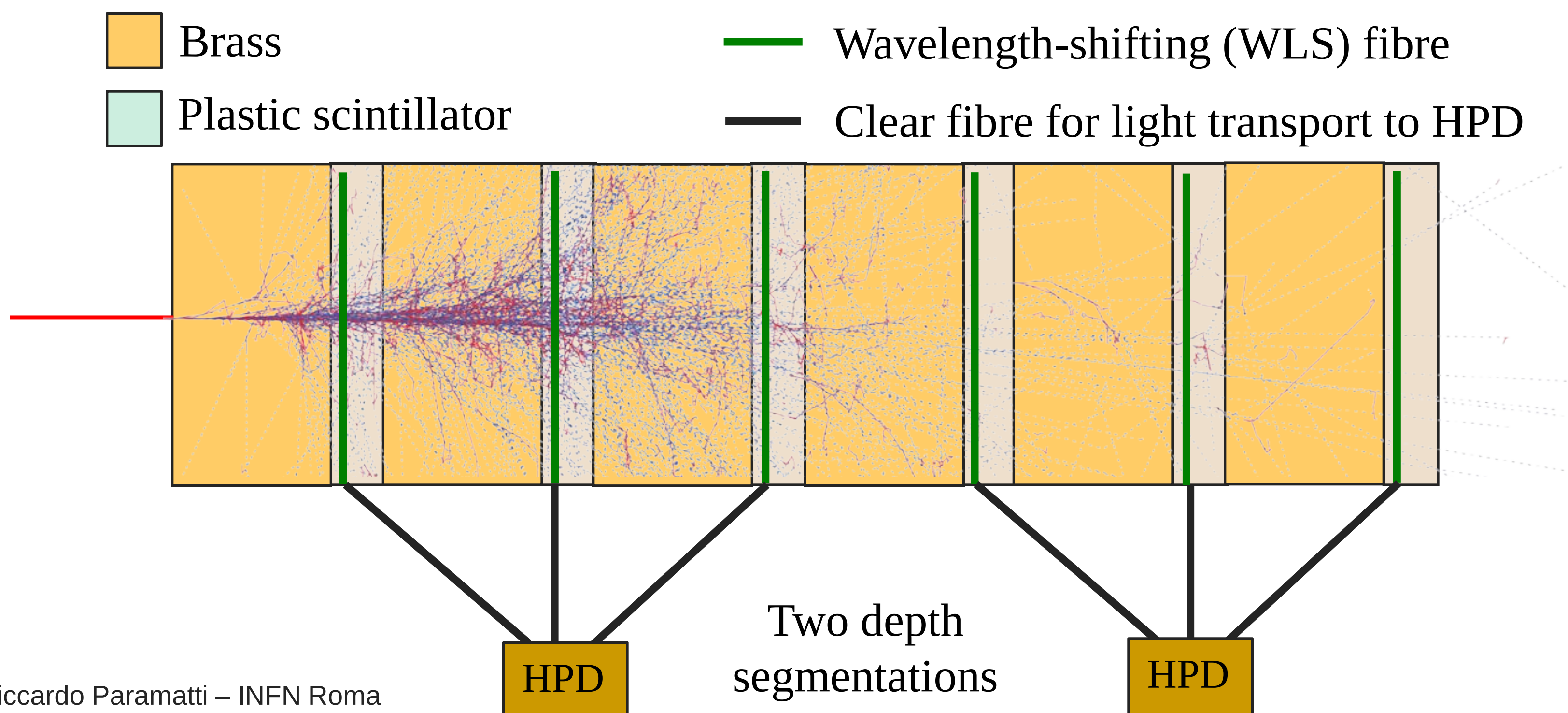

CMS Hadronic Calorimeter

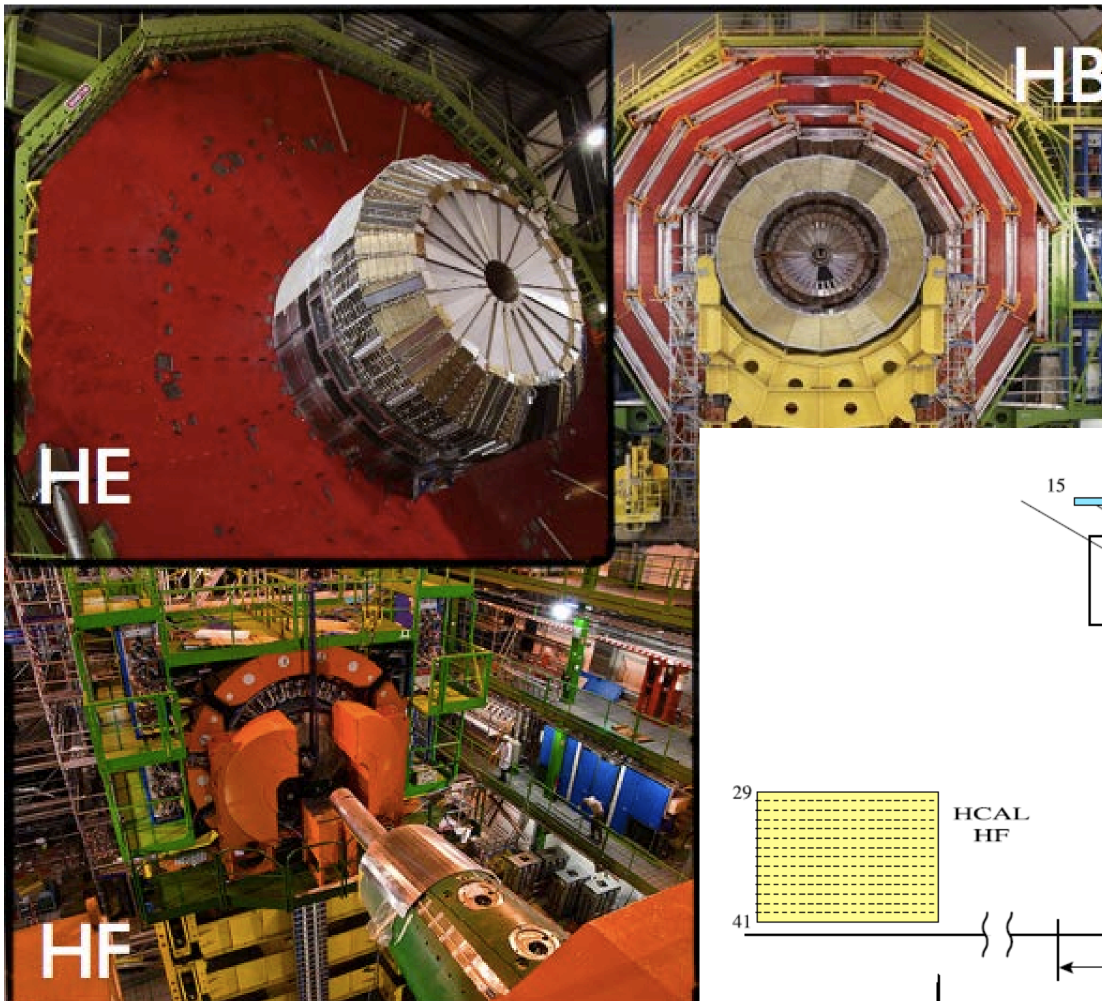

Detector	Readout	# Channels
HB/HE/HO	Hybrid Photo-Diode (HPD)	2592/2592/2160
HF	PMT	1728

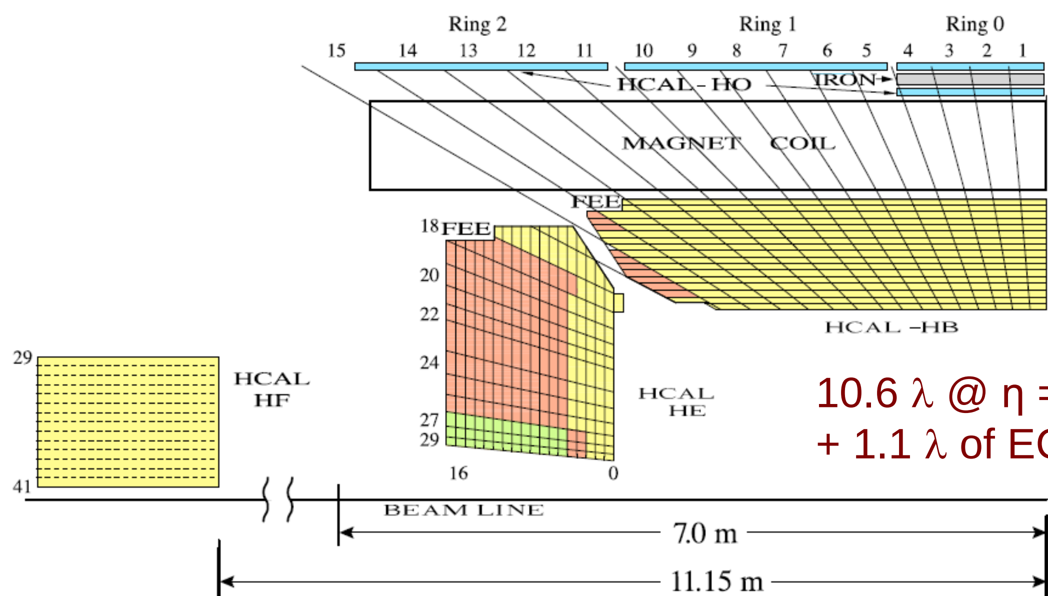

10.6 λ @ $\eta = 1.3$
+ 1.1 λ of ECAL

ECAL & HCAL locations in CMS

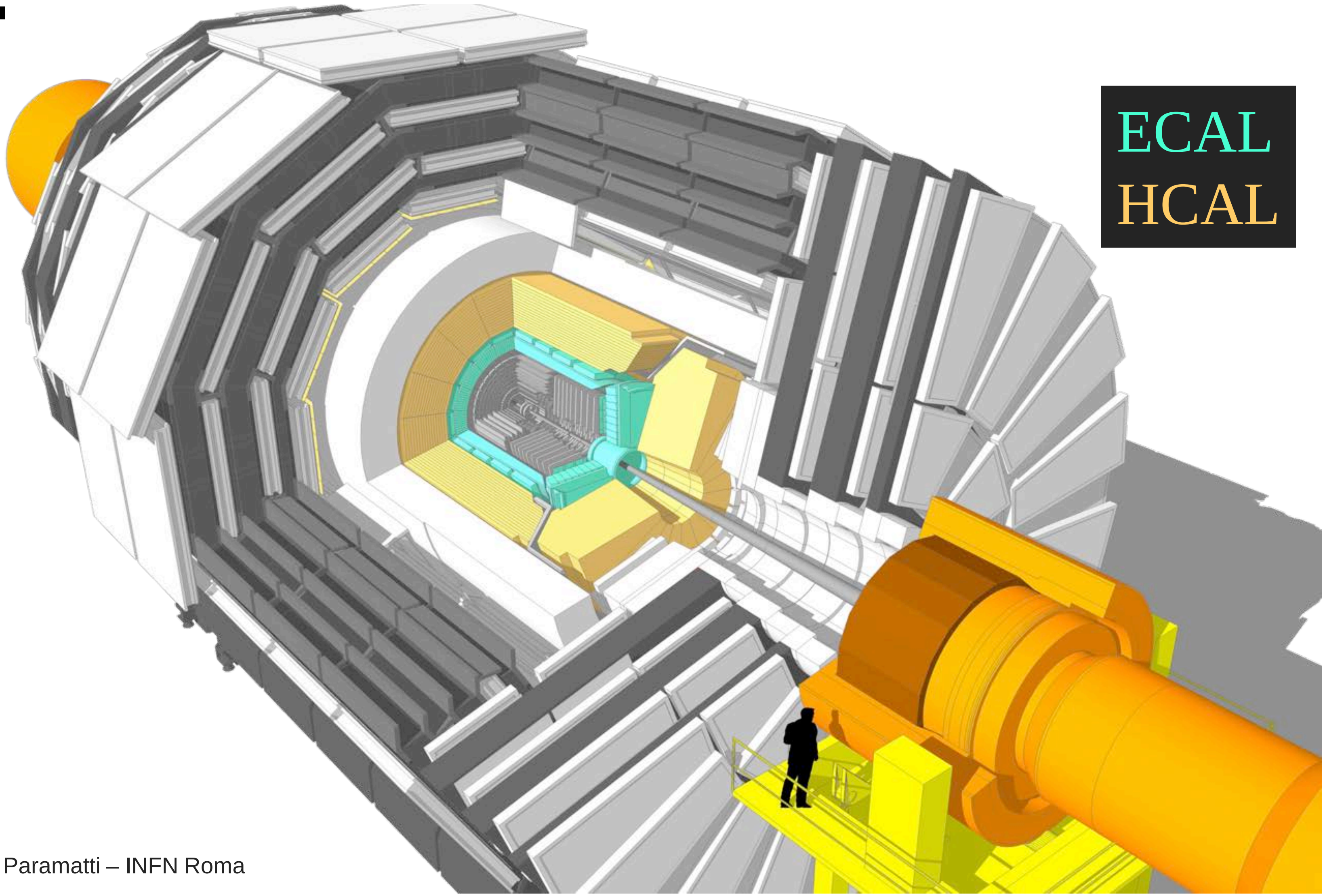

Construction and assembly of CMS calorimeters

Courtesy of
Dave Barney and
Pawel de Barbaro

EB/EE Crystals

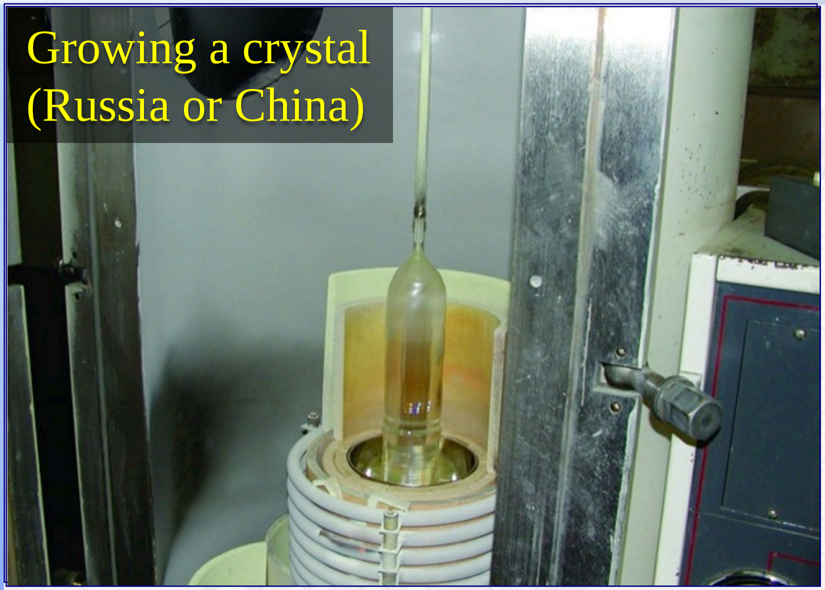

Growing a crystal (Russia or China)

Before and after cutting & polishing

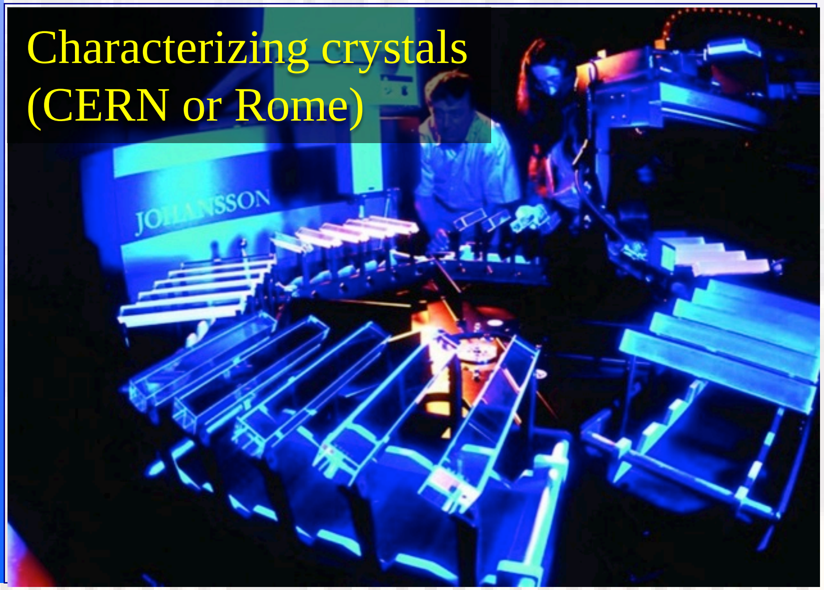

Characterizing crystals (CERN or Rome)

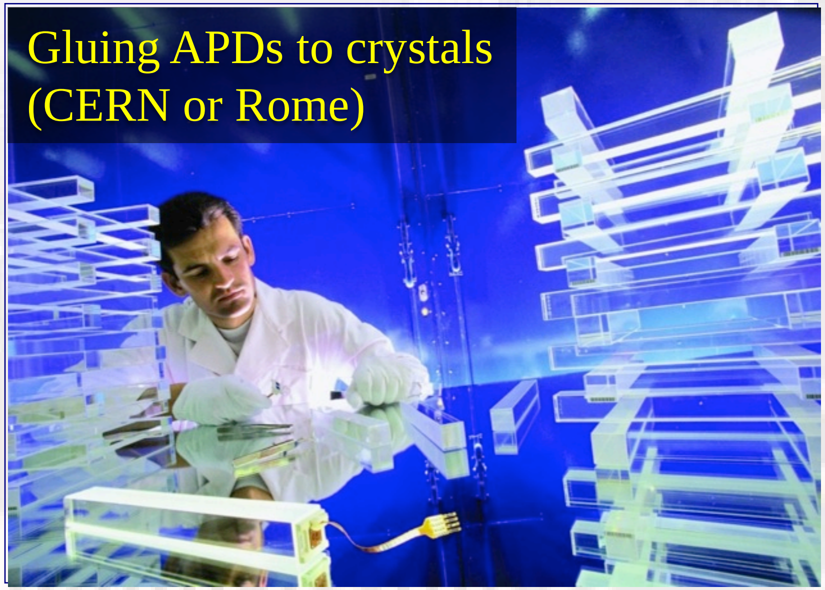

Gluing APDs to crystals (CERN or Rome)

D. Barney, P. de Barbaro

EB Assembly

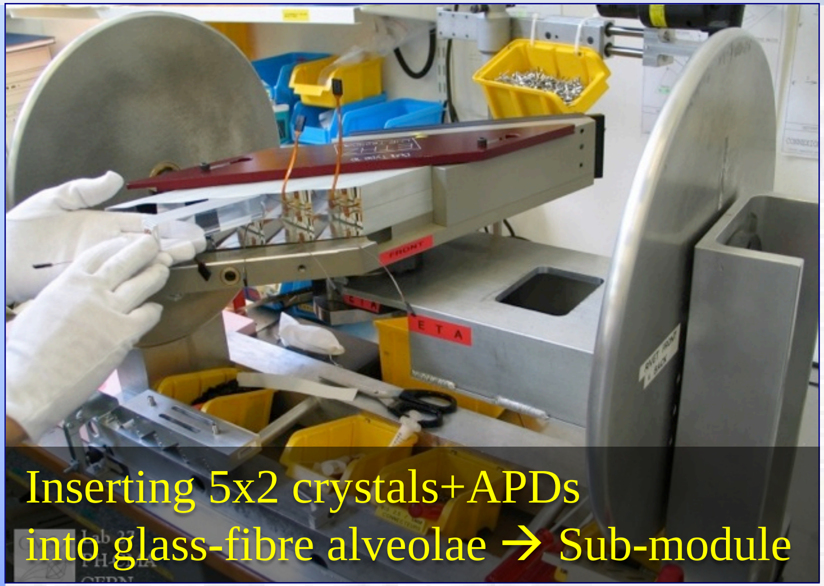

Inserting 5x2 crystals+APDs
into glass-fibre alveolae → Sub-module

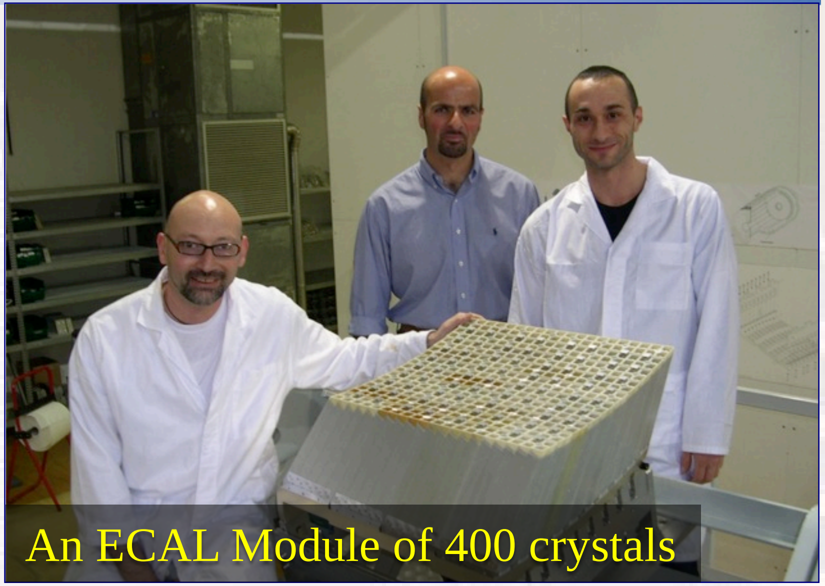

An ECAL Module of 400 crystals

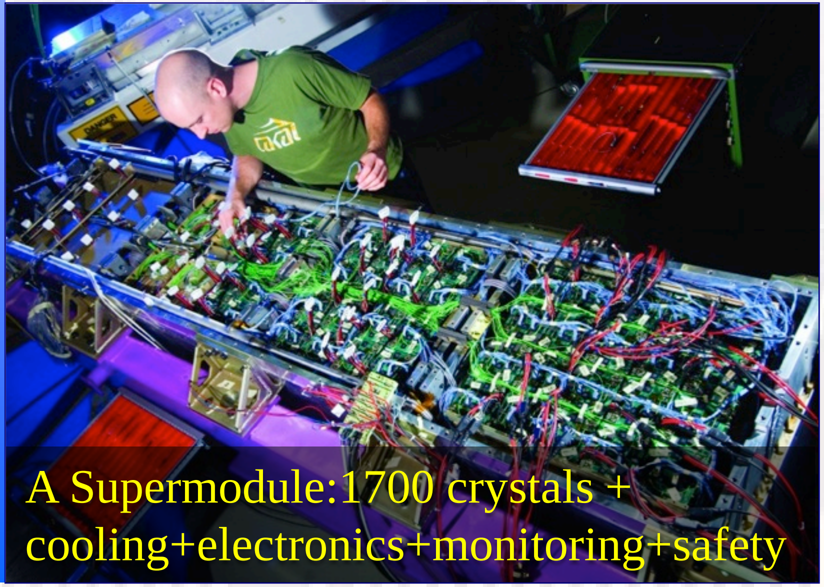

A Supermodule:1700 crystals +
cooling+electronics+monitoring+safety

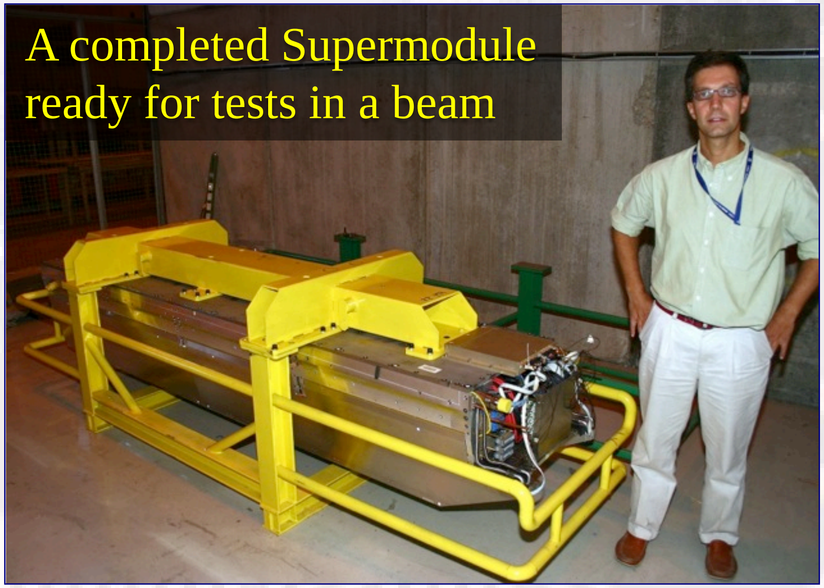

A completed Supermodule
ready for tests in a beam

EE Assembly

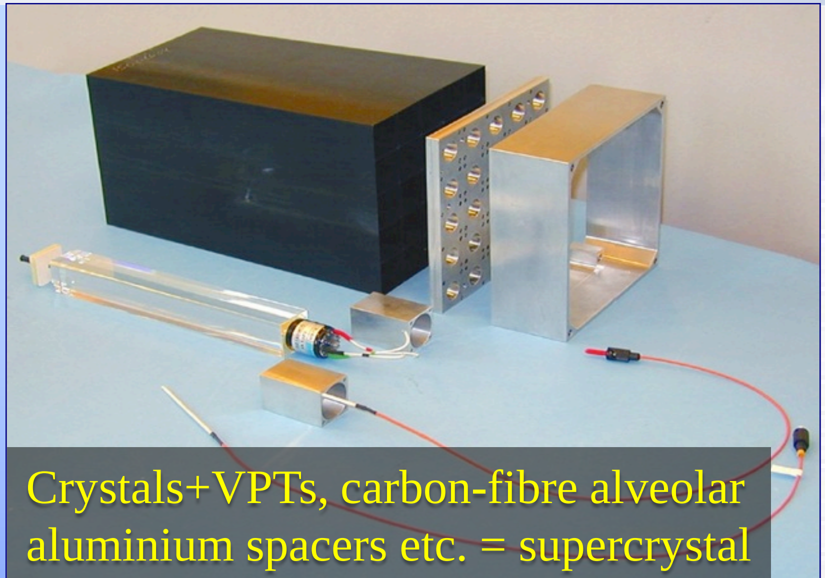

Crystals+VPTs, carbon-fibre alveolar aluminium spacers etc. = supercrystal

Trial installation of 5x5 supercrystals on a backplane

5x5 Supercrystals being mounted to form an EE Dee

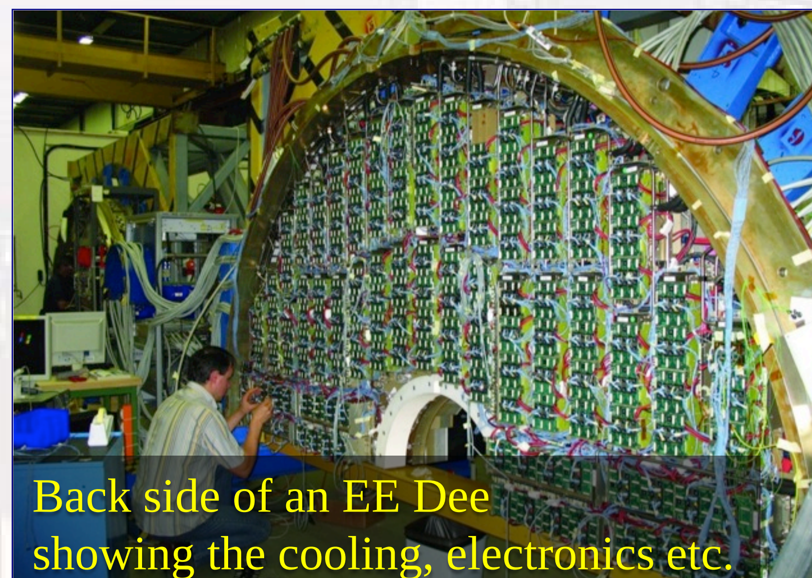

Back side of an EE Dee showing the cooling, electronics etc.

D. Barney, P. de Barbaro

ECAL Installation – 2007-2009

Installing barrel "supermodules" of 1700 crystals each

All 36 barrel supermodules installed - supported by HCAL barrel

Installing the endcap Preshower around the beam pipe

Installing one of four endcap ECAL Dees onto the HCAL Endcap

HB Assembly

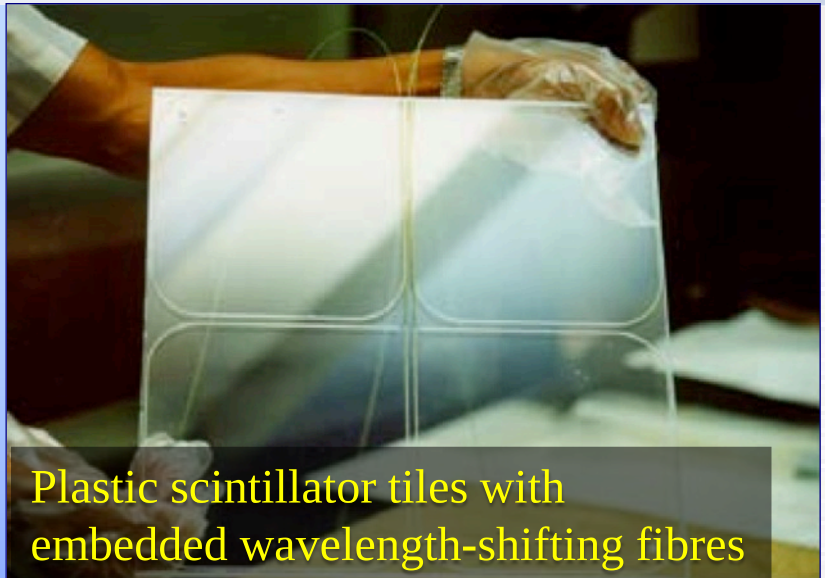

Plastic scintillator tiles with embedded wavelength-shifting fibres

One of 36 brass wedges showing gaps for the scintillators

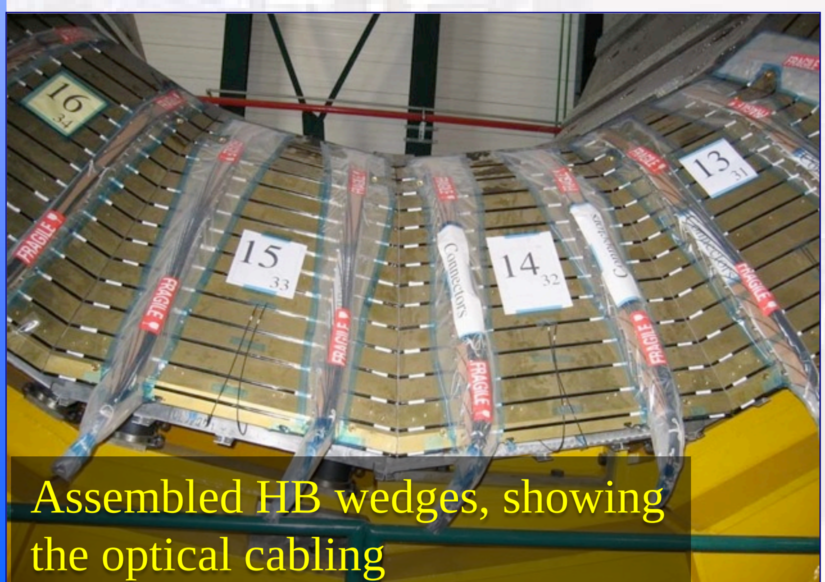

Assembled HB wedges, showing the optical cabling

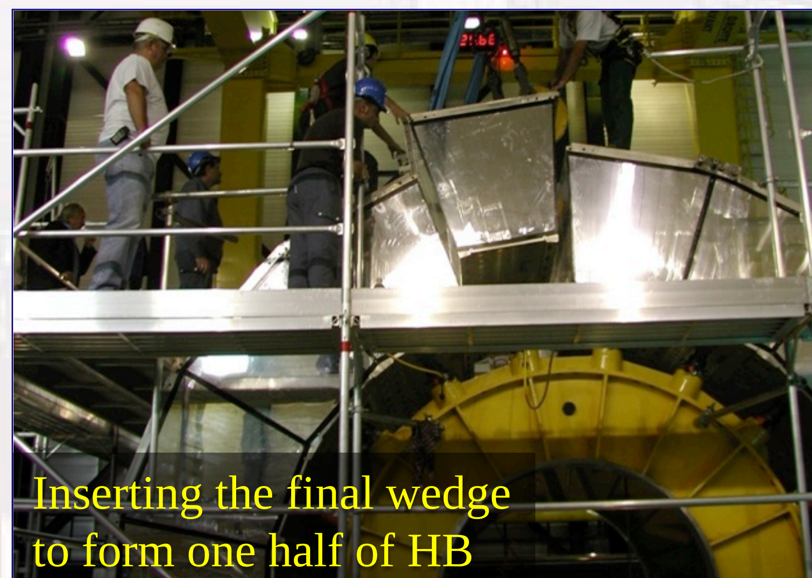

Inserting the final wedge to form one half of HB

D. Barney, P. de Barbaro

HE Construction


Brass for the HE came from Russian artillery shells


Melting the shells

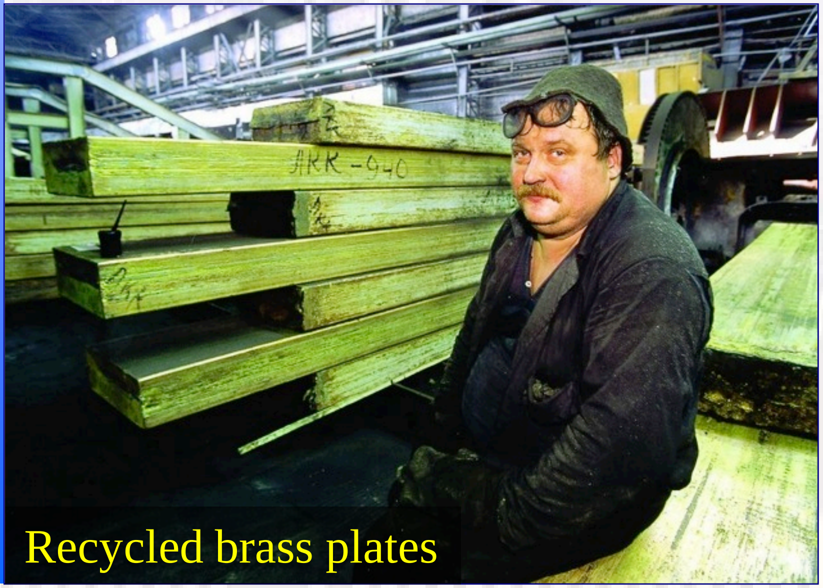

Recycled brass plates


Trial assembly of HE brass “petals”

HCAL Installation - 2007

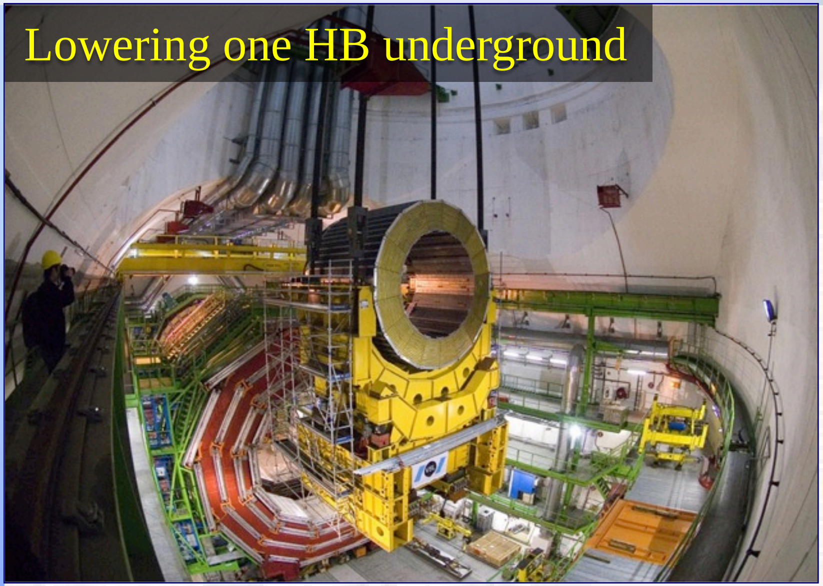
Lowering one HB underground


HB+ about to be inserted into YB0

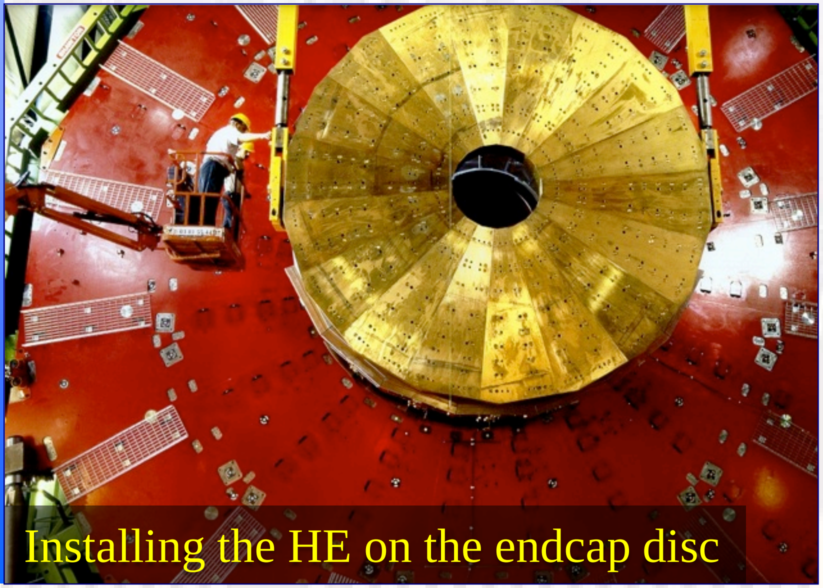
Installing the HE on the endcap disc

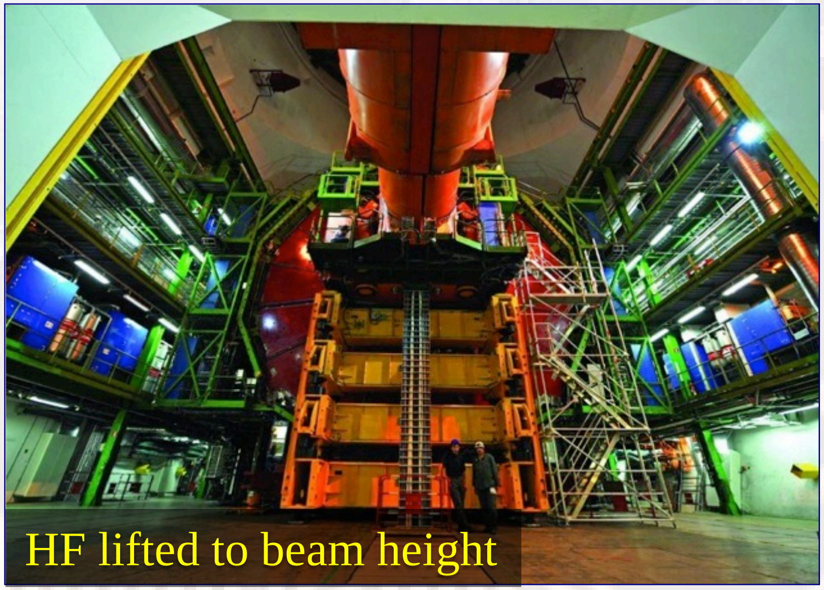
HF lifted to beam height

A general overview of HEP calorimeters

The Crystal Ball calorimeter

- 672 + 60 sodium iodide (NaI) crystals
- pioneering most of the features of modern calorimeters
- dedicated to the study of charmonium states

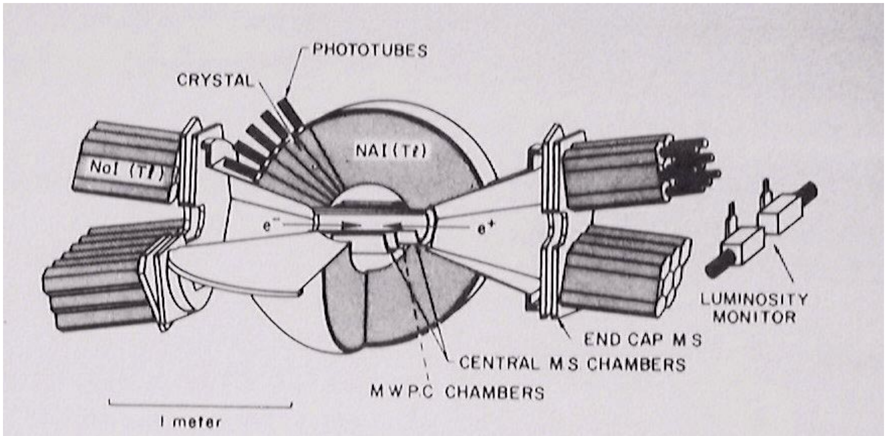

FIG. 2. Schematic of the detector.

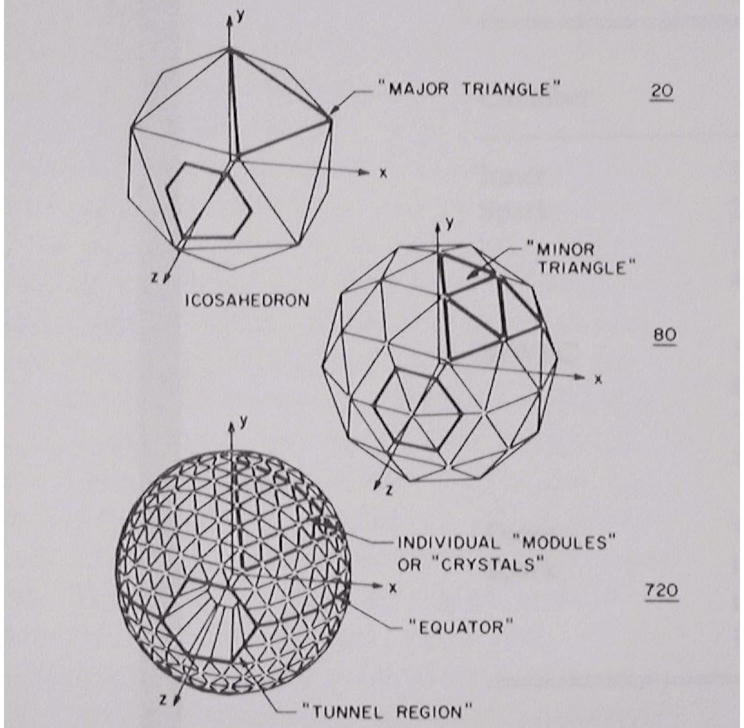

FIG. 3. Development of the ball geometry and nomenclature.

Tevatron calorimeters

- Proton-antiproton collider at $\sqrt{s} = 2$ TeV
- More time between bunch crossings and smaller dynamic range w.r.t. LHC constraints. No radiation hardness requirements.
- CDF:
  - ECAL $\rightarrow$ Lead/Scintillator
  - HCAL $\rightarrow$ Iron/Scintillator
- D0:
  - ECAL $\rightarrow$ Uranium/Liquid Argon
  - HCAL $\rightarrow$ Copper/Steel

Calorimeters at electron-positron colliders

- LEP collider $\sqrt{s}$ = 90-200 GeV
- L3:
  - ECAL BGO crystals
  - HCAL uranium/wire chambers
- OPAL:
  - ECAL lead glass
  - HCAL iron/streamer tube
- Aleph:
  - ECAL lead/wire chambers
  - HCAL iron/streamer tubes
- Delphi:
  - ECAL lead glass and HDPC
  - HCAL iron/streamer tubes

- Babar ECAL: CsI crystals
  - shorter w.r.t. L3 and CMS crystals because $\sqrt{s}$ = 10.58 GeV [m_Y(4S)]

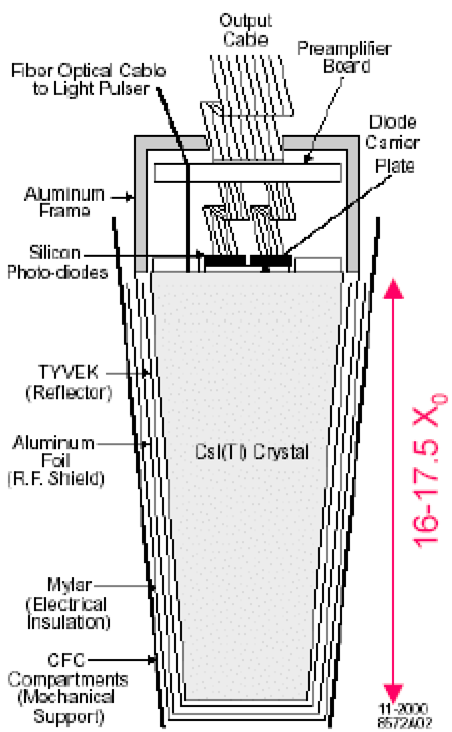

LHC calorimeters

- Atlas:
  - ECAL → Lead/Liquid Argon
  - HCAL → Steel/Plastic Scintillator Tiles
  - Forward → Copper & Tungsten/Liquid Argon
- LHCb:
  - ECAL → Lead/Scintillator
  - HCAL → Iron/Scintillator
- ALICE:
  - PHOS → $PbWO_4$ crystals
  - EMCAL → Lead/Scintillator

Atlas calorimeters

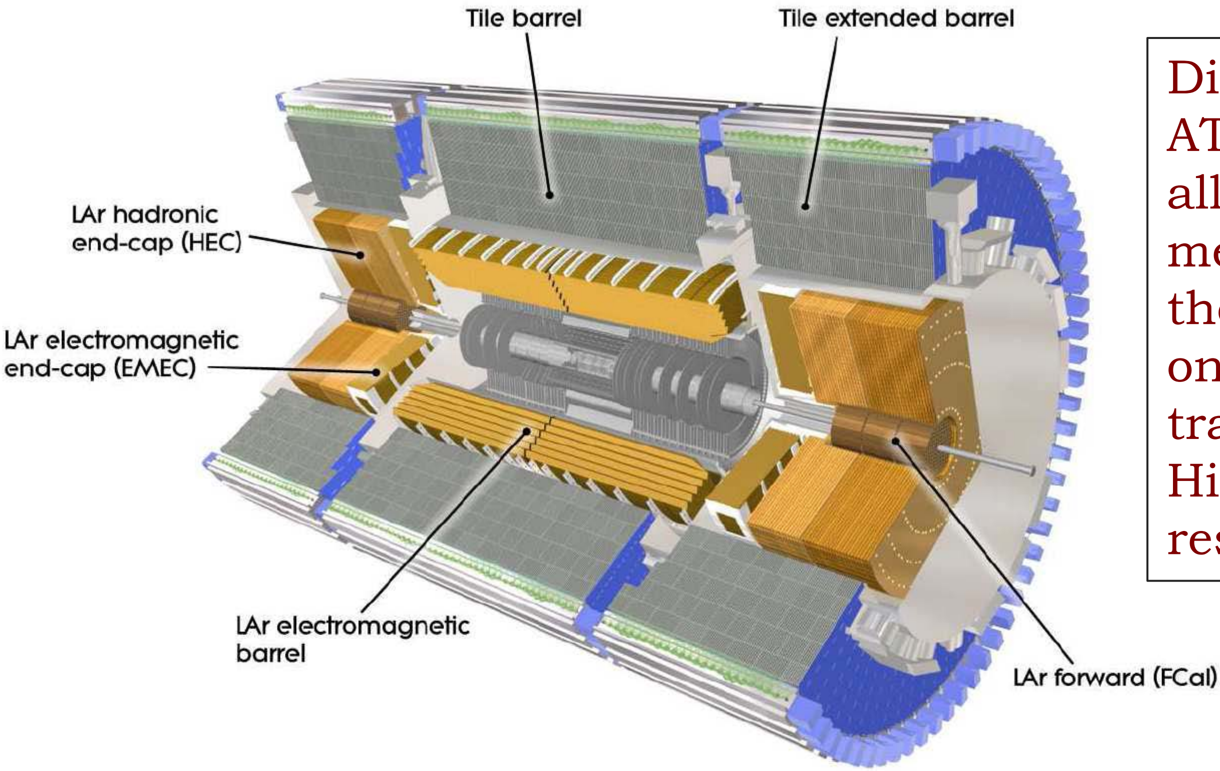

Different choices for ECALs: ATLAS sampling calorimeter allow to have redundant measurement of γ angle, while the measure of γ angle relies on vertex reconstruction from tracking in CMS.
Higher stochastic term with respect to CMS ECAL.

The choices made for the hadronic central section by ATLAS and CMS are similar: sampling calorimeters with scintillator as active material.
In both cases the dominant factor on resolution and linearity is the $e/h \neq 1$.
ATLAS higher segmentation and containment gives better energy resolution.

The Atlas LAr calorimeter

The Liquid Argon (LAr) calorimeter:
EM Barrel : ($|\eta|<1.475$) [Pb-LAr]
EM End-caps : $1.375<|\eta|<3.2$ [Pb-LAr]
Hadronic End-caps: $1.5<|\eta|<3.2$ [Cu-LAr]
Forward: $3.1<|\eta|<4.9$ [Cu,W-LAr]

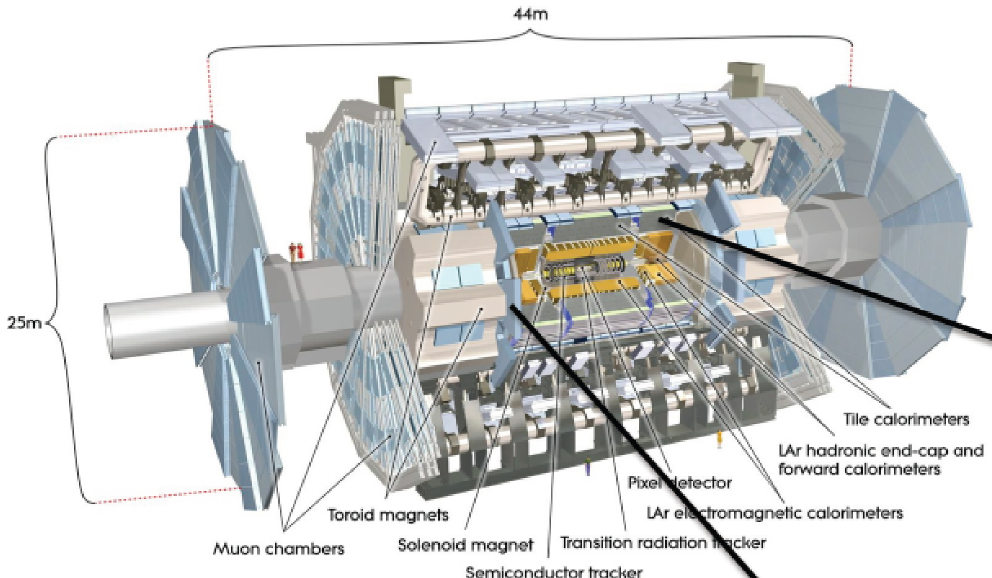

Fast & high granularity
Radiation resistance
Large dynamic range:
10 MeV → 3 TeV

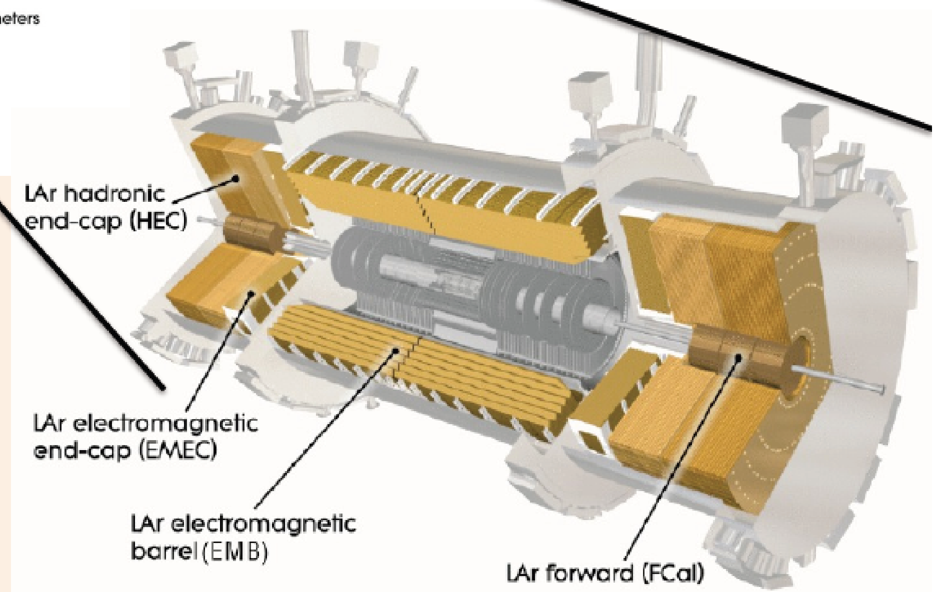

Electromagnetic (EM) calorimeter:
- Pb+LAr, accordion geometry
- high granularity 1st layer for $|\eta| \leq 2.4$

Presampler (PS) in front of accordion calorimeter for $|\eta| \leq 1.8$

182468 read-out channels in the whole LAr calorimeter
- 173312 in EM calorimeter (EMB + EMEC)

Working principle

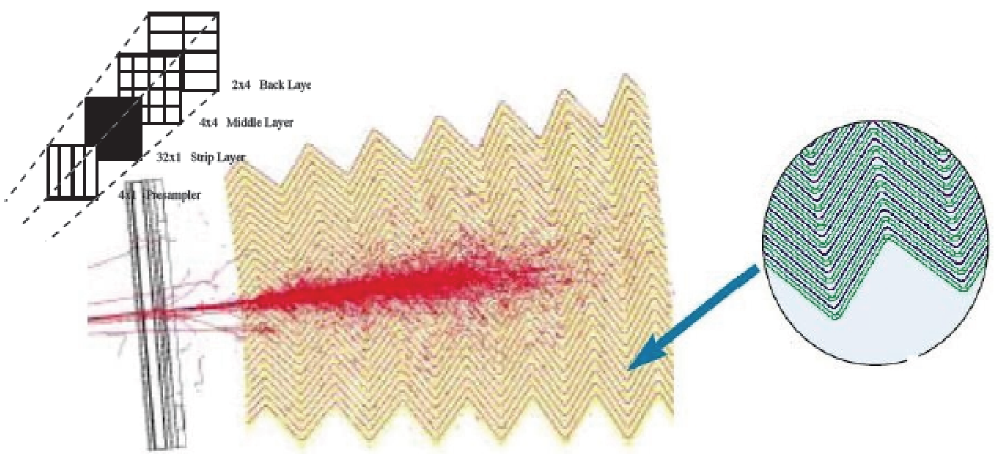

- **Accordion shape** in EM barrel and endcap calorimeters ($>22X_0$)
- **Sampling calorimeters** with Pb absorbers and active LAr gaps (2mm in barrel, 1.2 – 2.7mm in endcap)
- Incident electrons create **EM showers** in Pb (X_0=0.56cm) and LAr gaps (X_0=14.2cm)
  - secondary e^+ and e^- create e^-– ion pairs in LAr (W=23.3eV)
- Ionized electrons and ions drift in electric field (2kV

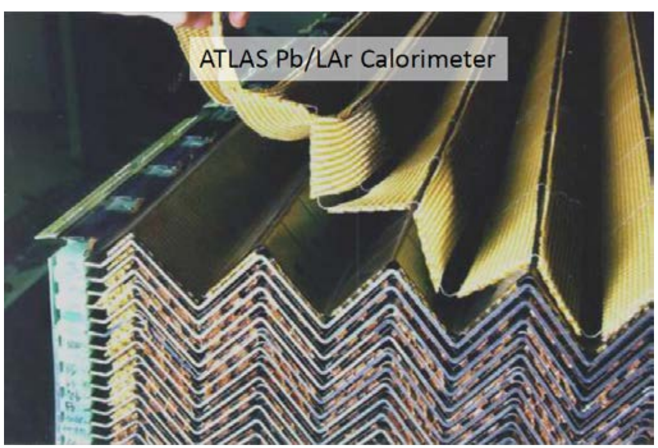

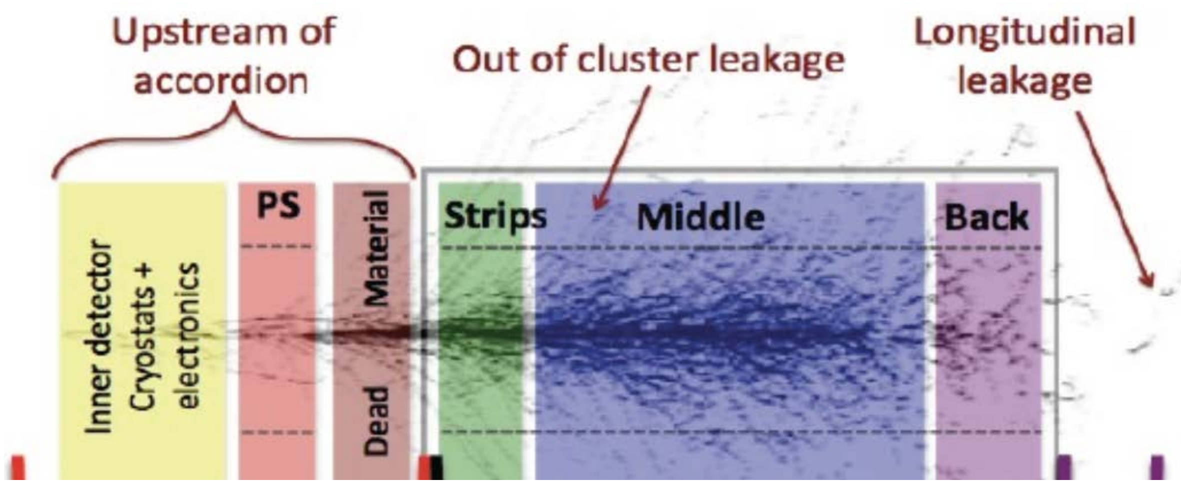

The accordion geometry

- The innovative accordion geometry of the e.m. part of the calorimeter provides fast, uniform response without azimuthal gaps.
- Three longitudinal layers + presampler
- Longitudinal dimension: ≈22 X0 = 47 cm (factor 2 w.r.t. CMS)

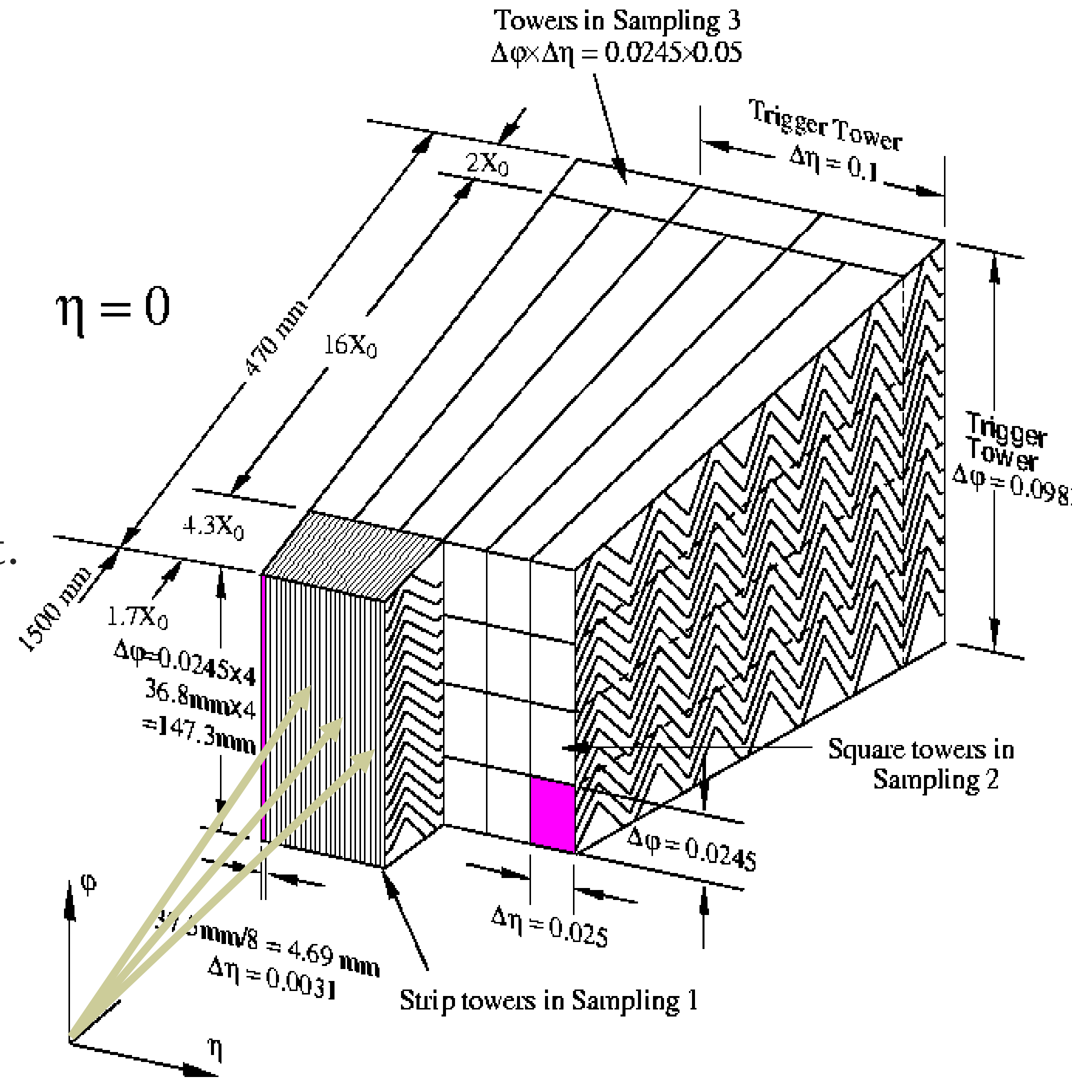

Mechanical uniformity is the challenge of this calorimeter: non uniformities modify electric field and detector response.

CMS vs Atlas ECAL

	ATLAS Lead/L. Ar ECAL		CMS PWO Crystal ECAL	
	Barrel	Endcaps	Barrel	Endcaps
# of Channels	110,208	83,744	61,200	14,648
Lateral Segmentation ($\Delta\eta \times \Delta\varphi$)				
Presampler	0.025 x 0.1			
Strip/Preshower	0.003 x 0.1	0.005 x 0.1		32 S /4 crystals
Main Body	0.025 x 0.025		0.0175 x 0.0175	Up to 0.05 x 0.05
Back	0.05 x 0.025			
Longitudinal Segmentation				
Presampler	10 mm L. Ar	2 x 2 mm L. Ar		
Strip/Preshower	~4.3 X_0	~4 X_0		3 X_0
Main Body	~16 X_0	~20 X_0	26 X_0	25 X_0
Back	~2 X_0	~2 X_0		
Designed Energy Resolution				
Stochastic: a	10%	10 - 12%	2.7%	5.7%
Constant: b	0.7%	0.7%	0.55%	0.55%
Noise: C	0.25 GeV	0.25 GeV	0.16 GeV	0.77 GeV

The ATLAS HCAL

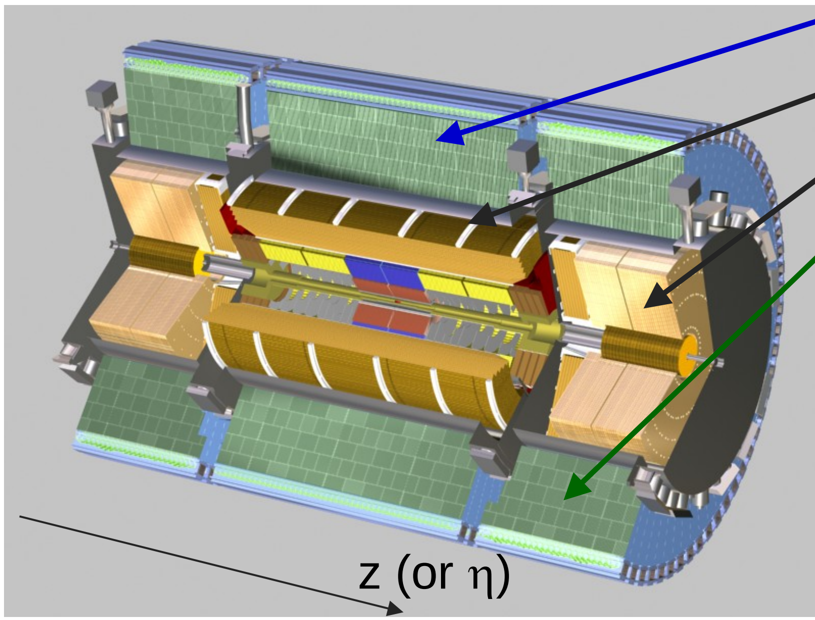

Hadronic Tiles Barrel
(Liq Arg EM calorimeter cryostat)
(Forward calorimeters cryostats)
Hadronic Tiles Extended barrel

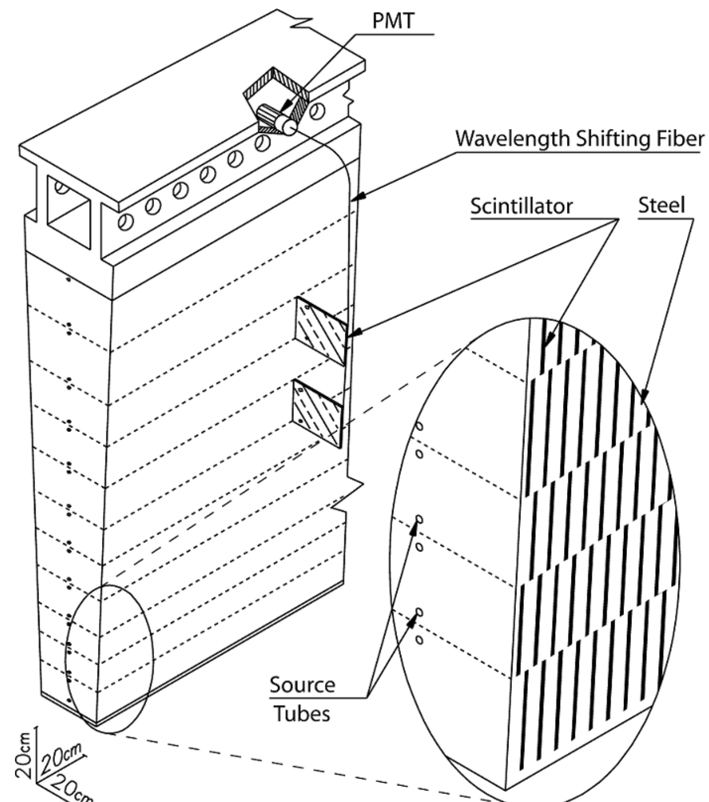

- Tiles perpendicular to beam axis
- 3 longitudinal layers
- Wavelength shifting fibers carry light to PMTs
- Covers $|\eta|<1.7$

Atlas vs CMS HCAL

More interaction lengths in Atlas, especially in the barrel region.

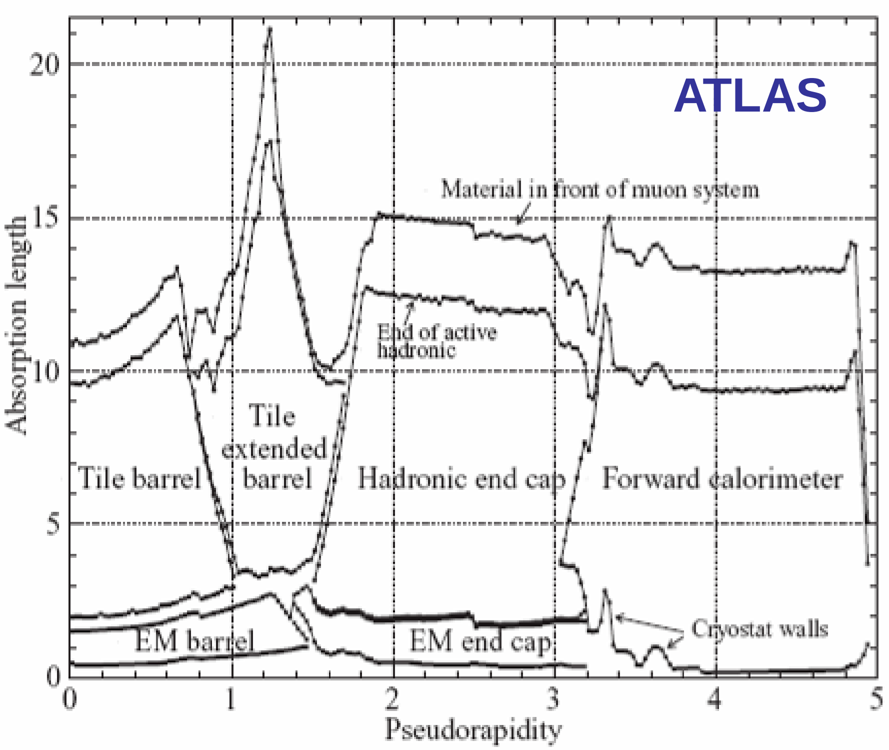

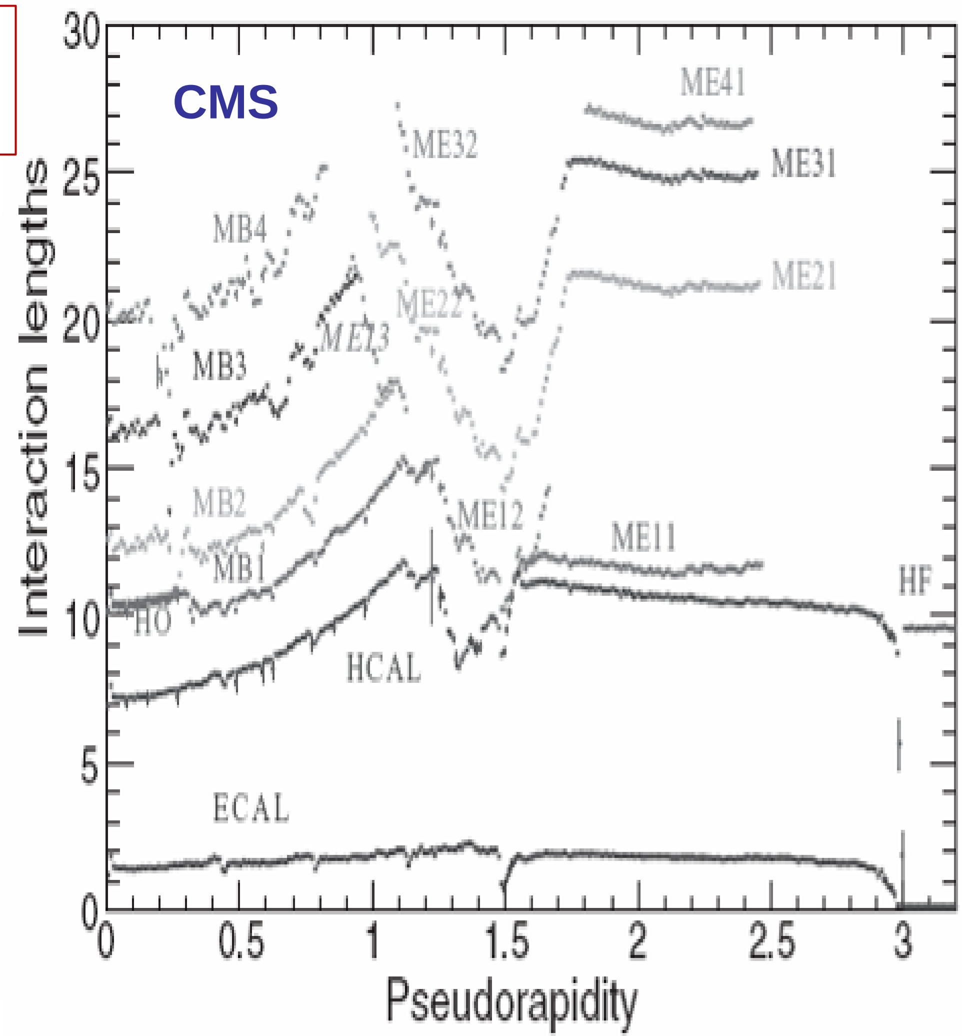

Electromagnetic calorimeter performance

Crystal quality measurements

Automatic Crystals Quality Control Systems

for reception tests

- Automatic processing of crystals in sets of 5 on a tray, also used for storage and capsule gluing
- Measurements of dimensions by a standard 3D machine
- Light yield on several points (uniformity)
- Transmission (lateral on several points, longitudinal)

+ spot checks of radiation tolerance

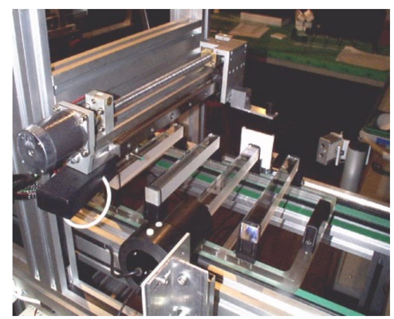

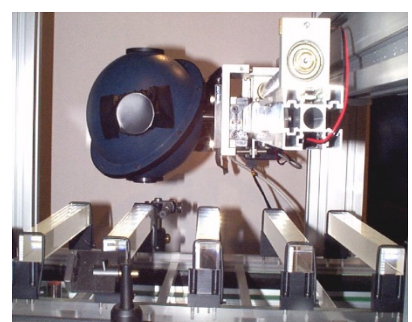

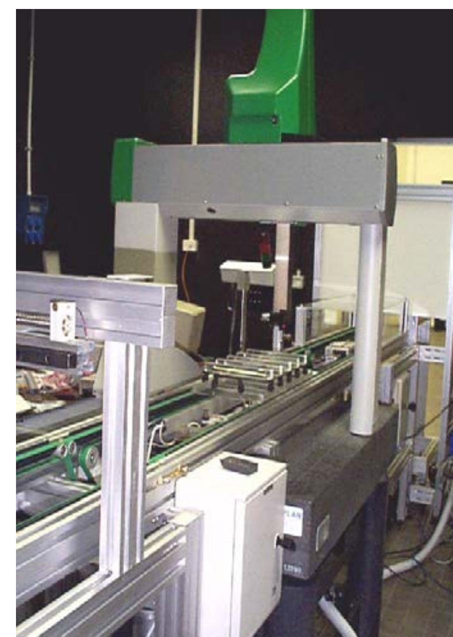

Pre-calibration Campaign

A very intense 10 years long pre-calibration campaign. Several orders of magnitude in energy: from 1 MeV of Co^{60} source to 120 GeV electron beam.

Laboratory measurements during crystal qualification phase.

(2000-2006)

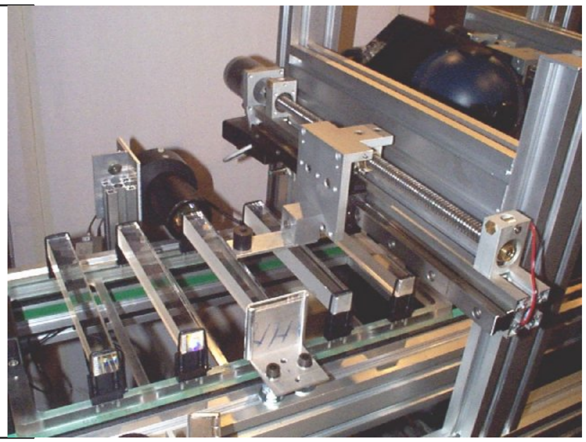

Test Beam: Cern electron beams.

From 15 GeV to 250 GeV.

(2004-2007)

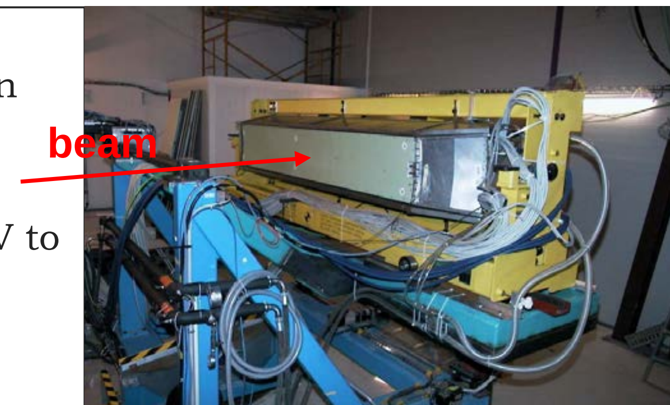

Channel intercalibration with cosmic muons (only Barrel SMs)

(2006-2007)

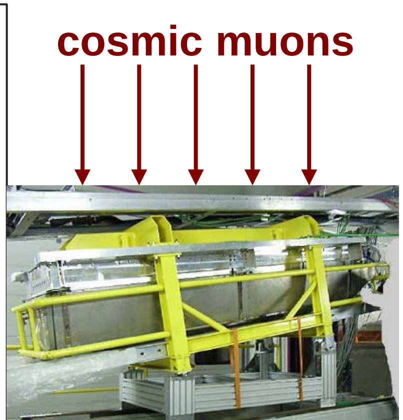

Beam Splash:
In September 2008 and November 2009, beam was circulated in LHC, stopped in collimators 150m away from CMS

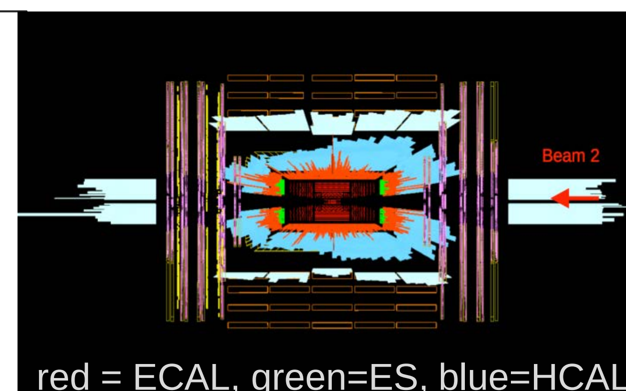

ECAL «standalone» energy resolution

- ECAL «standalone» energy resolution measured at the test beam: (3x3 arrays of barrel crystals in the absence of magnetic field, with no material in front of the calorimeter and negligible inter-calibration contribution in the constant term)

$$\frac{\sigma(E)}{E} = \frac{2.8\%}{\sqrt{E(GeV)}} \oplus \frac{0.128}{E(GeV)} \oplus 0.3\%$$

- Results used to tune MC simulation.
- In-situ, for unconverted photons with energies in the range of interest for physics analyses, ~100 GeV, the in-situ constant term dominates.
- Constant term in-situ strongly depends on the quality of the stability, calibration and monitoring.
- Asymptotically to be kept at ~0.5%

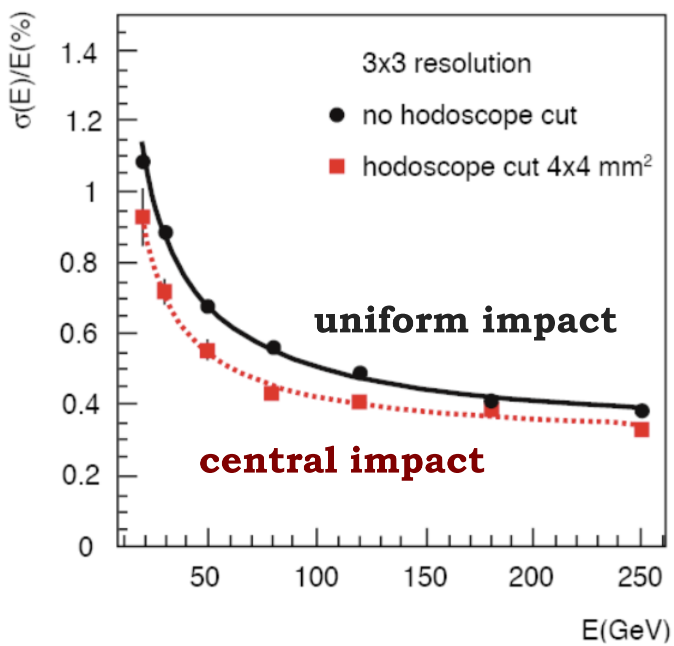

ECAL stability

- Fraction of working channels during LHC Run1: EB 99.1%, EE 98.4% (0.5% recovered in LS1) ES 96.8% (3.1% recovered in LS1)

- Temperature stability:
  - crystal light yield and APD gain are temperature dependent.
  - negligible contribution to the energy resolution constant term if temperature of the Barrel/Endcap stable within 0.05 °C/0.1 °C (VPT are stable in temperature).

Temperature stability of the ECAL Barrel and Endcap detectors.

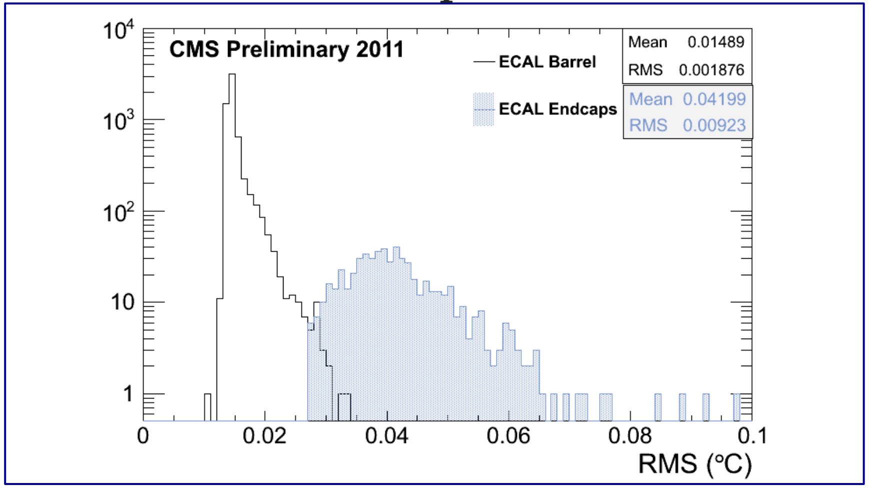

- High Voltage stability (EB):
  - APD gain very sensitive to the bias voltage: 3%/Volt
  - Stability < 60 mV is required to provide a negligible contribution to the constant term of the energy resolution.
  - High Voltage stability well within allowed limits

e/γ energy reconstruction in ECAL

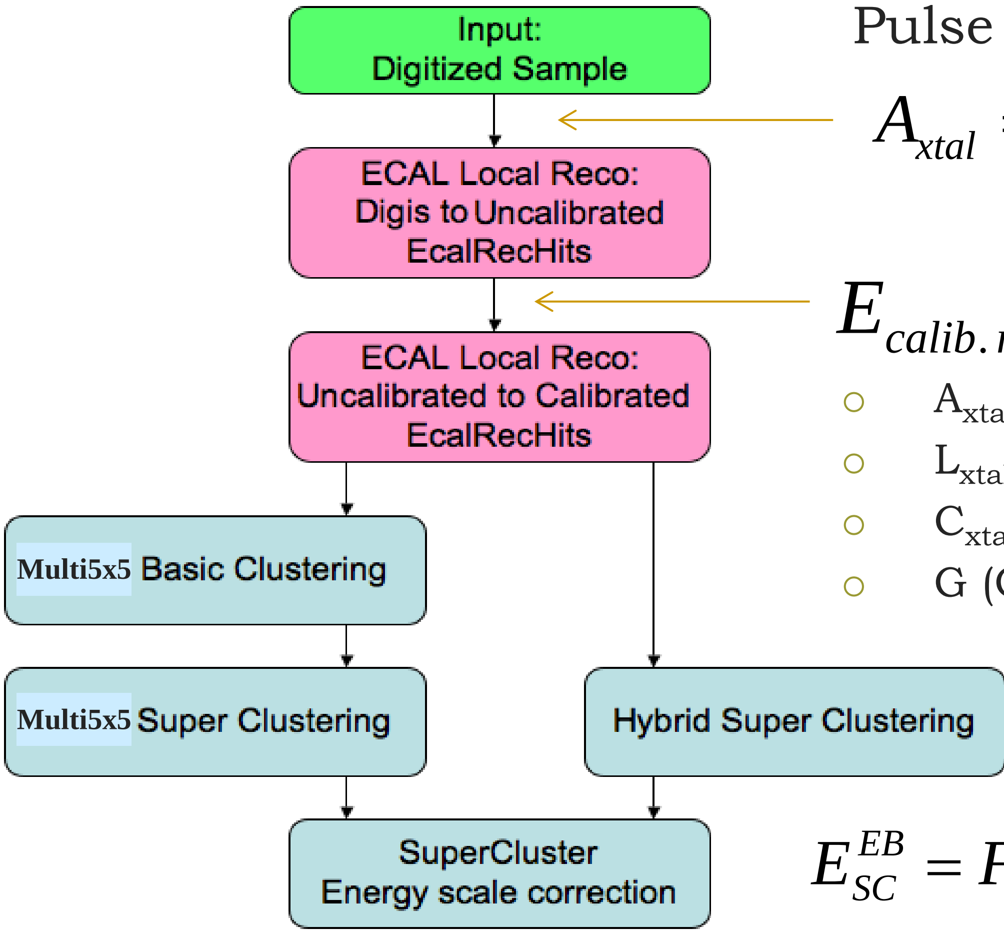

Pulse amplitude reconstruction:

$$A_{xtal} = \sum_{time\ sample\ i} (w_i \cdot s_i)$$

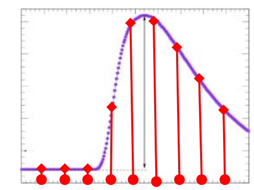

$$E_{calib.recHit} = G \cdot C_{xtal} \cdot L_{xtal}(t) \cdot A_{xtal}$$

- A_{xtal} (ADC counts) → uncalibrated RecHit
- L_{xtal} (time dependent) → laser correction.
- C_{xtal} ($\langle C_{xtal} \rangle = 1$) → channel inter-calibration
- G (GeV/ADC) → EB and EE scale.

$$E_{SC}^{raw} = \sum_{SC\ xtals} E_{calib.recHit}$$

$$E_{SC}^{EB} = F(\eta, \sigma_\phi / \sigma_\eta, E_\perp) \cdot E_{SC}^{raw}$$

$$E_{SC}^{EE} = F(\eta, \sigma_\phi / \sigma_\eta, E_\perp) \cdot \left(E_{SC}^{raw} + E_{ES}\right)$$

e/γ energy reconstruction in ECAL

Measurement of electron/photon energy:

$$E_{e,\gamma} = F_{e,\gamma} \cdot \sum_{xtal} \left(G \cdot C_{xtal} \cdot L_{xtal}(t) \cdot A_{xtal}\right)$$

- A_{xtal} [ADC counts] → signal channel amplitude
- L_{xtal} → laser monitoring correction (time dependent)
- C_{xtal} → crystal inter-calibration ($\langle C_{xtal} \rangle = 1$)
- G [GeV/ADC] → ECAL energy scale
- Σ →e.m. shower, energy deposited over several crystals clustered with dynamic algorithms
- F → cluster energy corrections
  - particle dependent
  - compensate shower leakage and bremsstrahlung losses for electrons

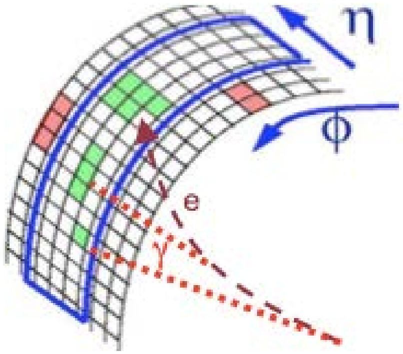

The evaluation of above contributions in the next slides

ECAL response monitoring

Radiation ⇒ Wavelength-dependent loss of light transmission (w/o changes in scintillation)

Crystal Transparency ***drops*** within a run by a few percent but ***recovers*** in the inter-fill periods

- Inject fixed amount of light to monitor transparency loss
- Response loss up to 5% in EB and up to 60% in EE (25% in the electron acceptance region |η| < 2.5)

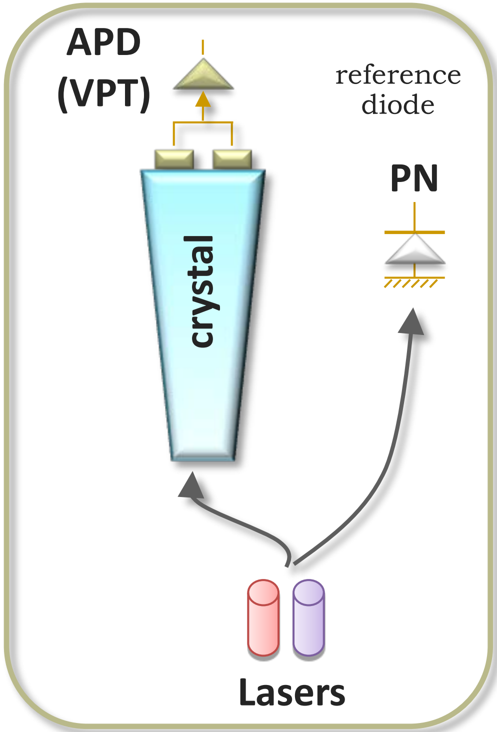

Cycle of response loss during irradiation and recovery in beam-off periods

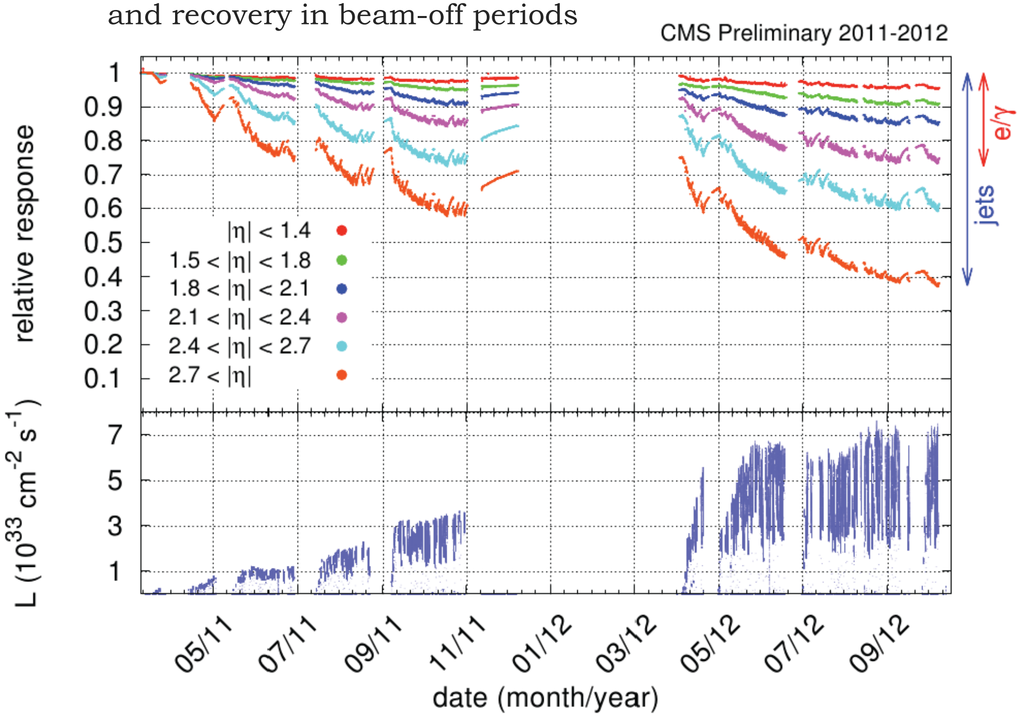

ECAL response stability

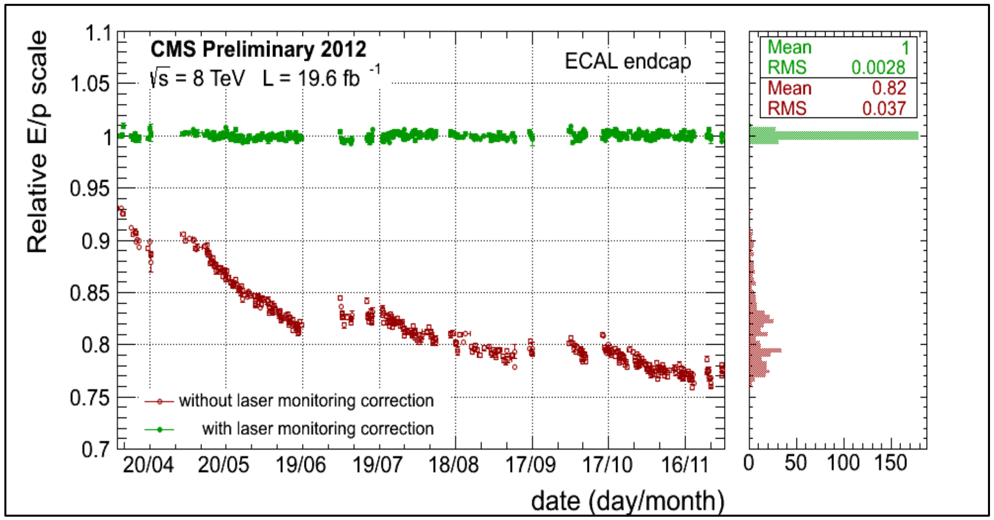

Stability of the energy scale after monitoring corrections with Weν events.

- Barrel: average signal loss ~5%
  RMS stability ~0.1%
- Endcaps: average signal loss ~25%
  RMS stability ~0.3%

Stability of the ECAL resolution from Zee invariant mass peak.

- Barrel: resolution stable within errors.
- Endcaps: worsening of ~1.5% in quad. (residual PU effect)

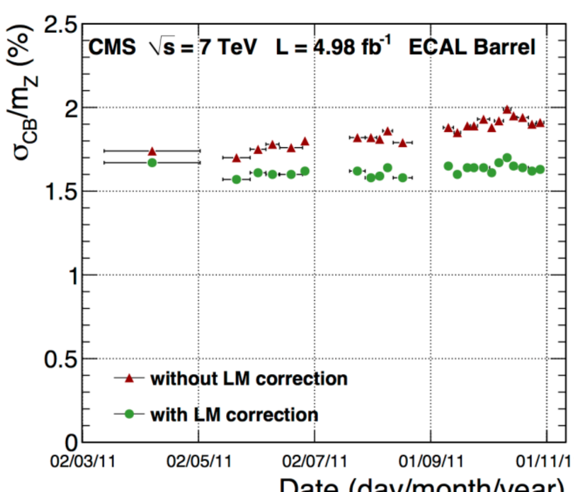

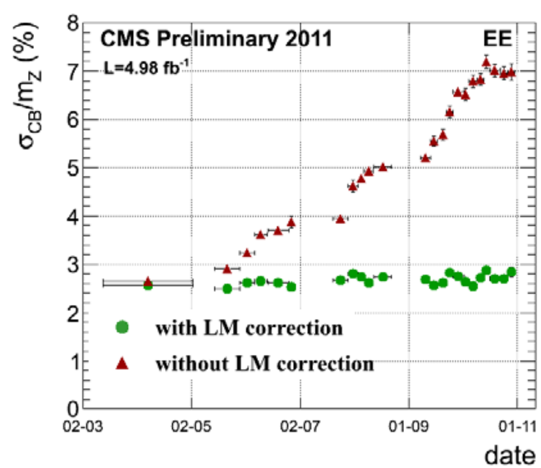

Crystal inter-calibration

- Several methods to calibrate (and follow-up) in-situ:
  - **φ-symmetry calibration**: invariance around the beam axis of energy flow in minimum bias events. Intercalibrate crystals at the same pseudorapidity.
  - **π^0 and η calibration**: mass constraint on photon energy, use unconverted γ's reconstructed in 3x3 matrices of crystals.
  - **High energy electron** from W and Z decays (E/p with single electrons and invariant mass with double electrons).

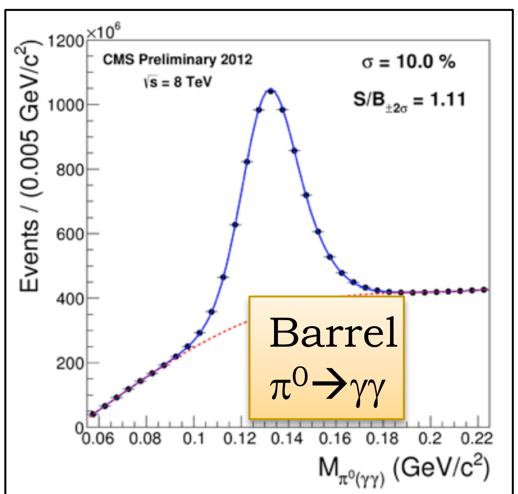

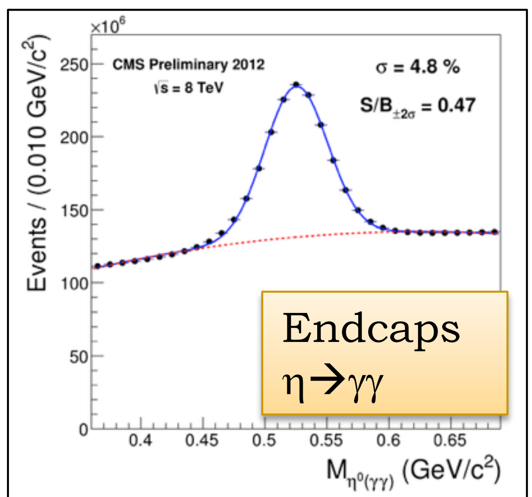

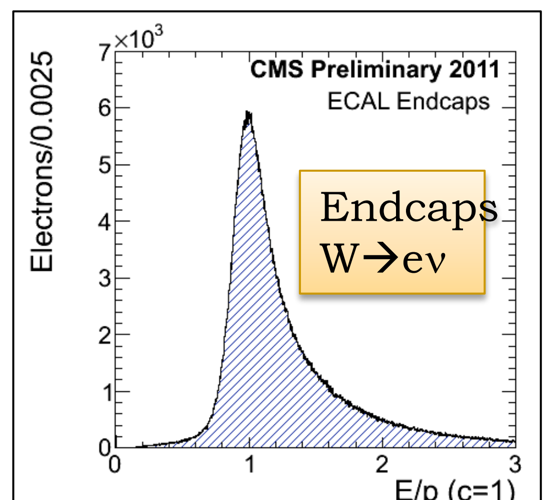

Crystal inter-calibration

combining all calibration methods

Barrel: <1% (~0.4% for |η|<1)
Endcaps: ~2% (almost everywhere)

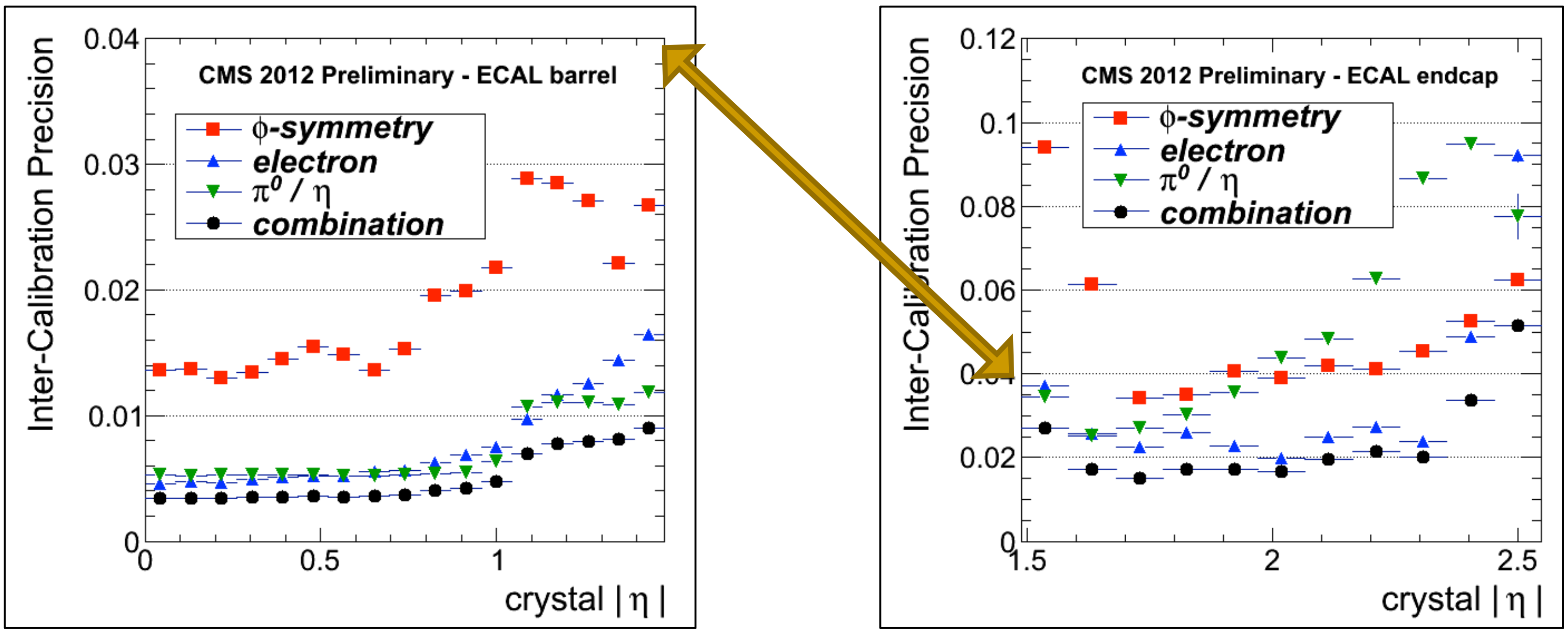

- **φ-symmetry calibration**: limited by systematic uncertainties
- **π^0 and η calibration**: limited by systematic uncertainties
- **high energy electron:** statistically limited for |η|>1

ECAL Calibration

- Zee invariant mass distribution applying :
  - channel Inter-Calibration
  - IC and Laser Monitoring corrections

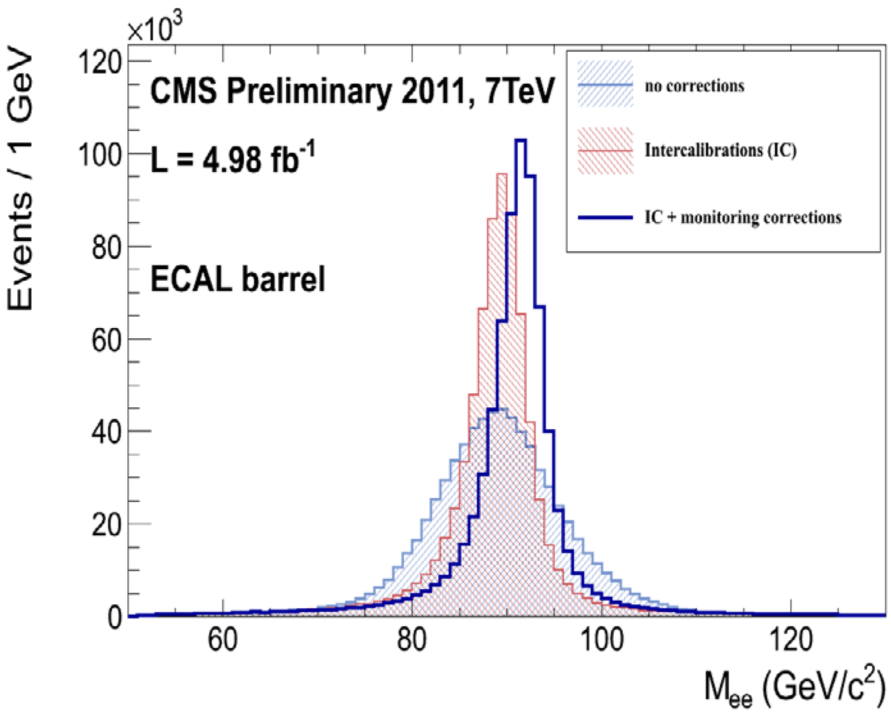

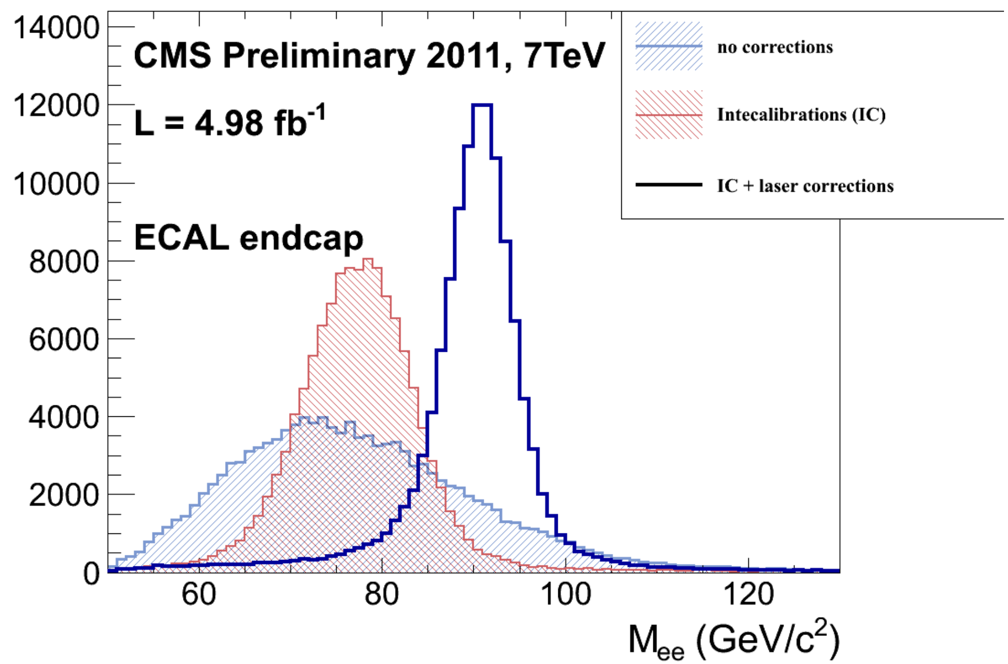

Alignment (in time and space)

- Timing fundamental in exotic long lived particle searches and in anomalous signal rejection.
- Time difference between the seed crystals for the two Z electrons.
- The time resolution for a single ECAL crystal, for the energy range of electrons from Z decays, is 0.19/0.28 ns in EB/EE.
- No longitudinal segmentation of ECAL → Photon direction from shower position and identification of the interaction vertex
- Relative alignment of the ECAL crystals and the CMS tracker measured using electrons from Z→ee and W→eν events.
- Position resolution ≤ 1 mm

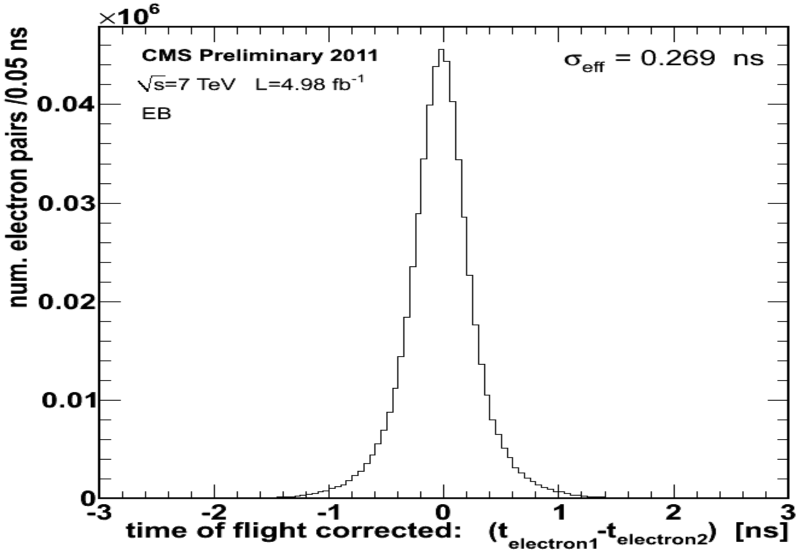

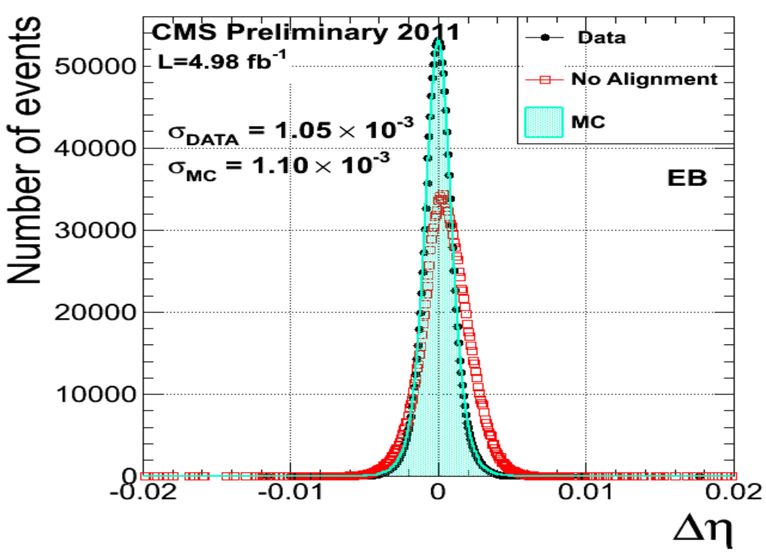

Tracker material

- Complex tracking system + frames + cooling + cables and services
- Up to two radiation lengths between the interaction point and the electromagnetic calorimeter !
- Bremsstrahlung and photon conversions (fraction of the e/γ energy not reaching the calorimeter).

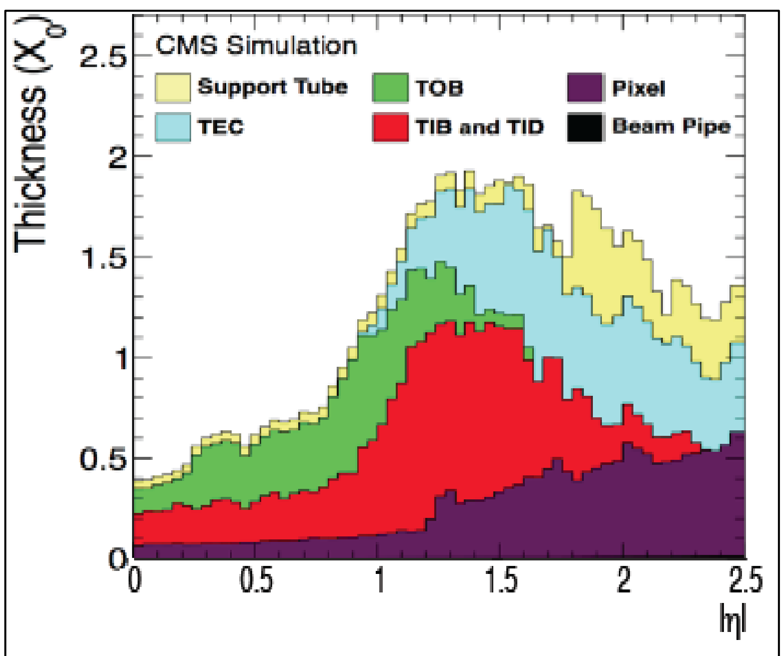

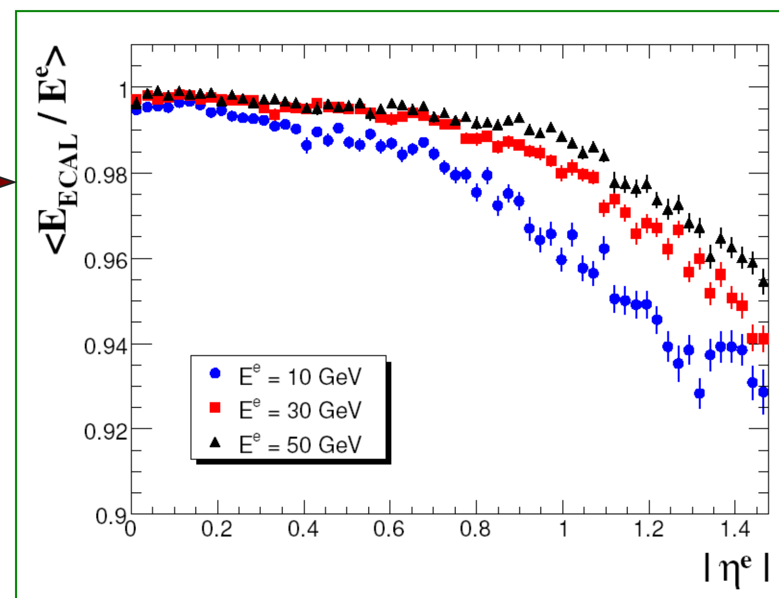

Cluster Energy Corrections

Cluster Energy corrections vs pseudo-rapidity for non-showering and showering electrons.

- compensate for unclustered energy and energy not reaching the calorimeter: strongly related to the amount of material in front of ECAL.
- energy lost inside gaps: intermodule boundary visible in the Barrel

Use R_9 shower-shape variable to discriminate:

- low / high bremsstrahlung electrons
- unconverted / converted photons

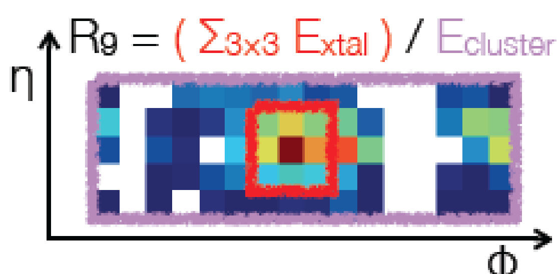

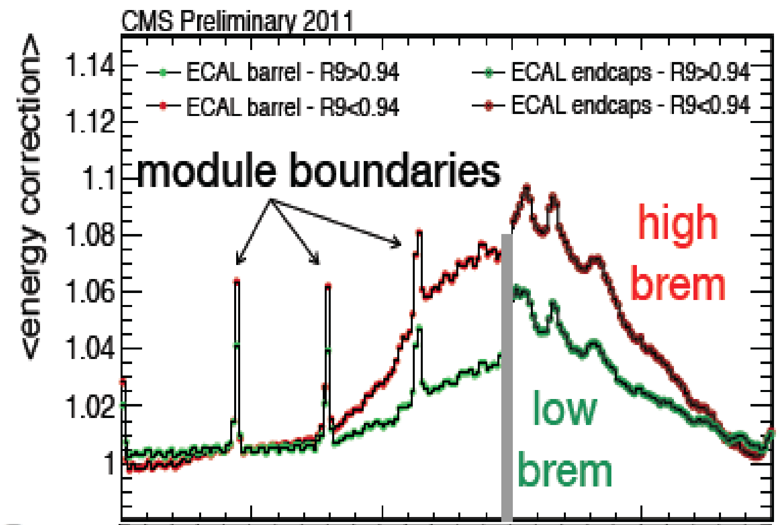

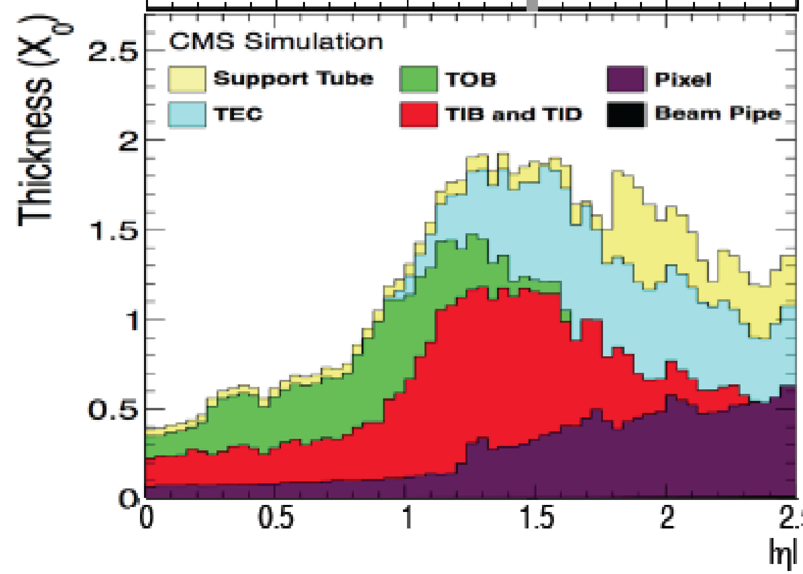

Optimal clustering

- Zee invariant mass distribution with optimal ECAL clustering

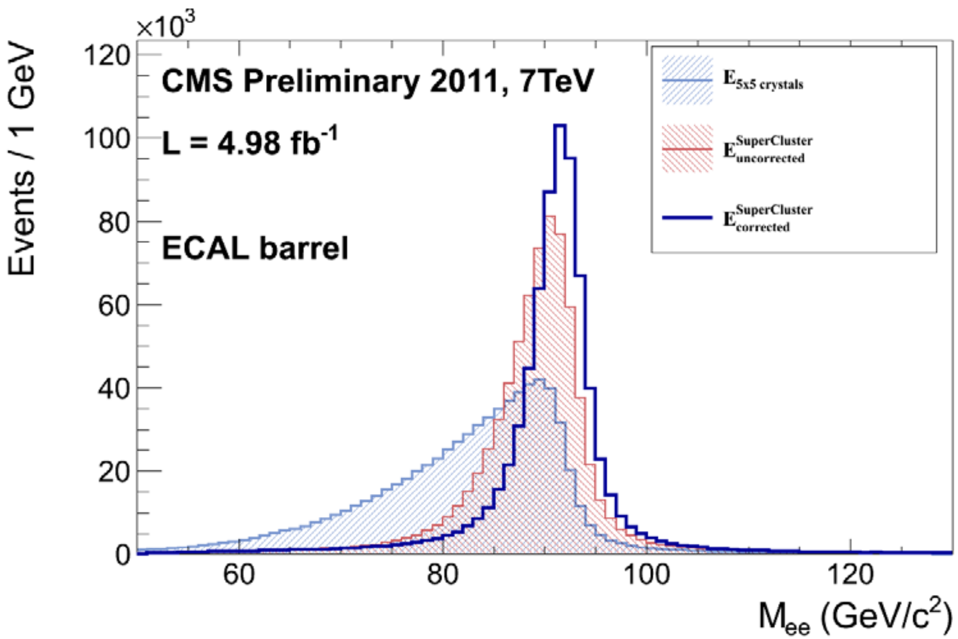

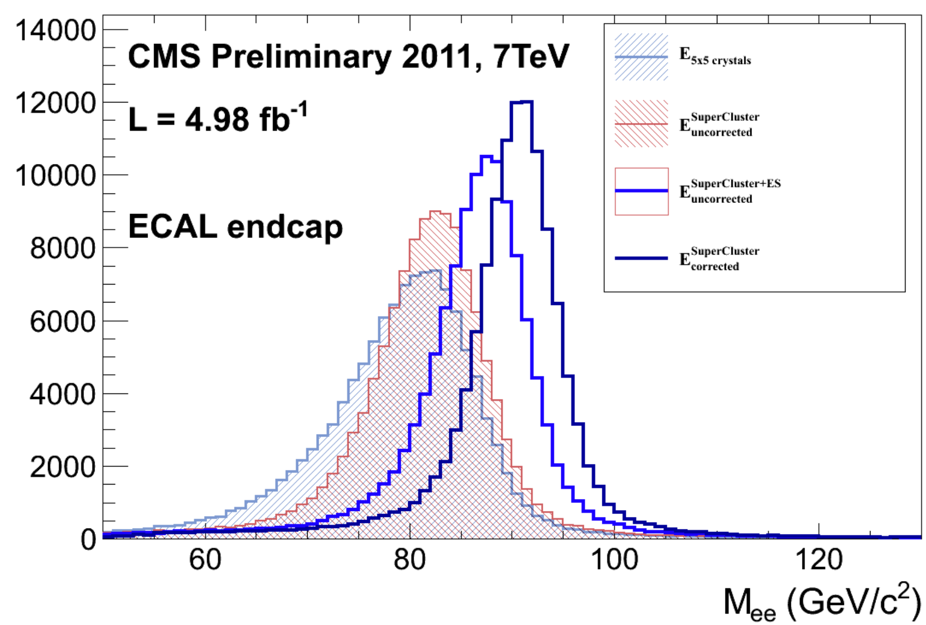

Data – MC comparison of energy resolution

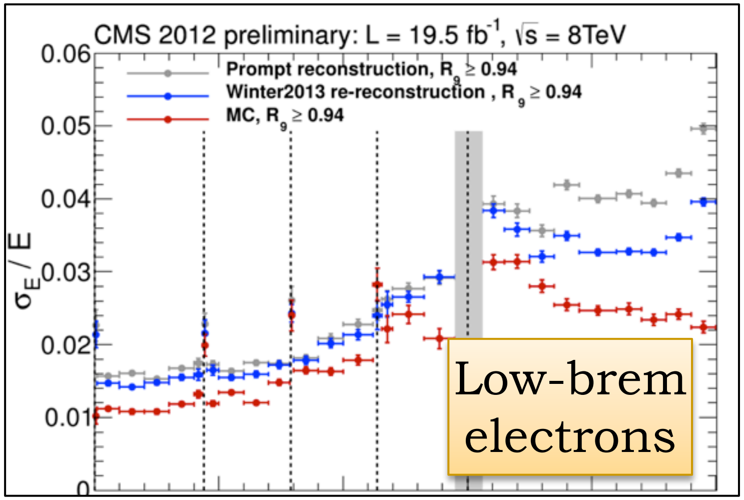

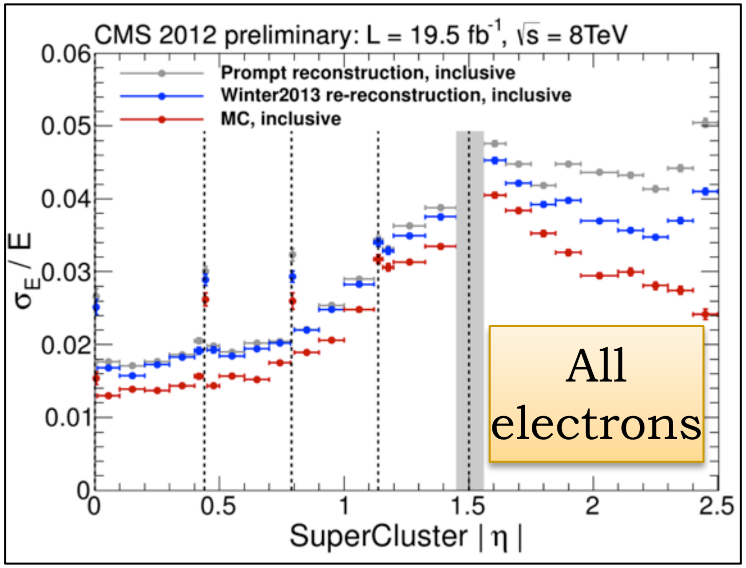

Double effort continuously ongoing to:

1. Improve the energy resolution both in Data and MC: inter-calibration precision, optimization of cluster corrections.
2. Reduce the difference between data and MC due to contributions possibly not fully simulated (laser correction stability, tuning of the material simulation, etc).

A perfect simulation of all the cables and services is a mission impossible !

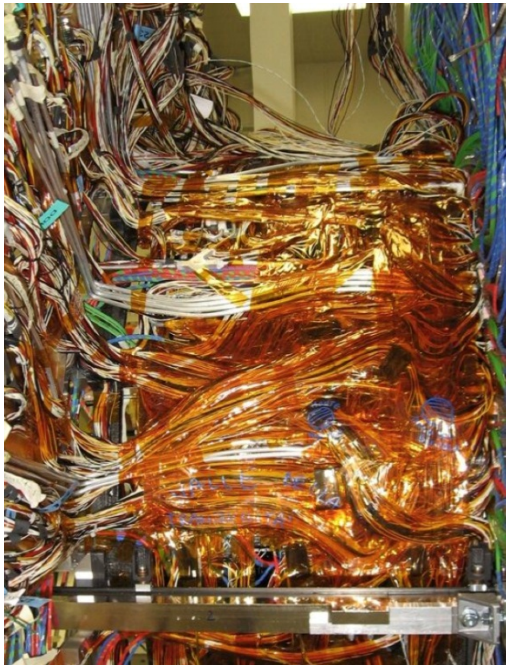

Ultimate tuning of energy resolution in simulation

- Simulation adapted by adding an extra smearing term (as a function of pseudo-rapidity, shower shape and transverse momentum)
- After this final correction, the agreement is excellent.

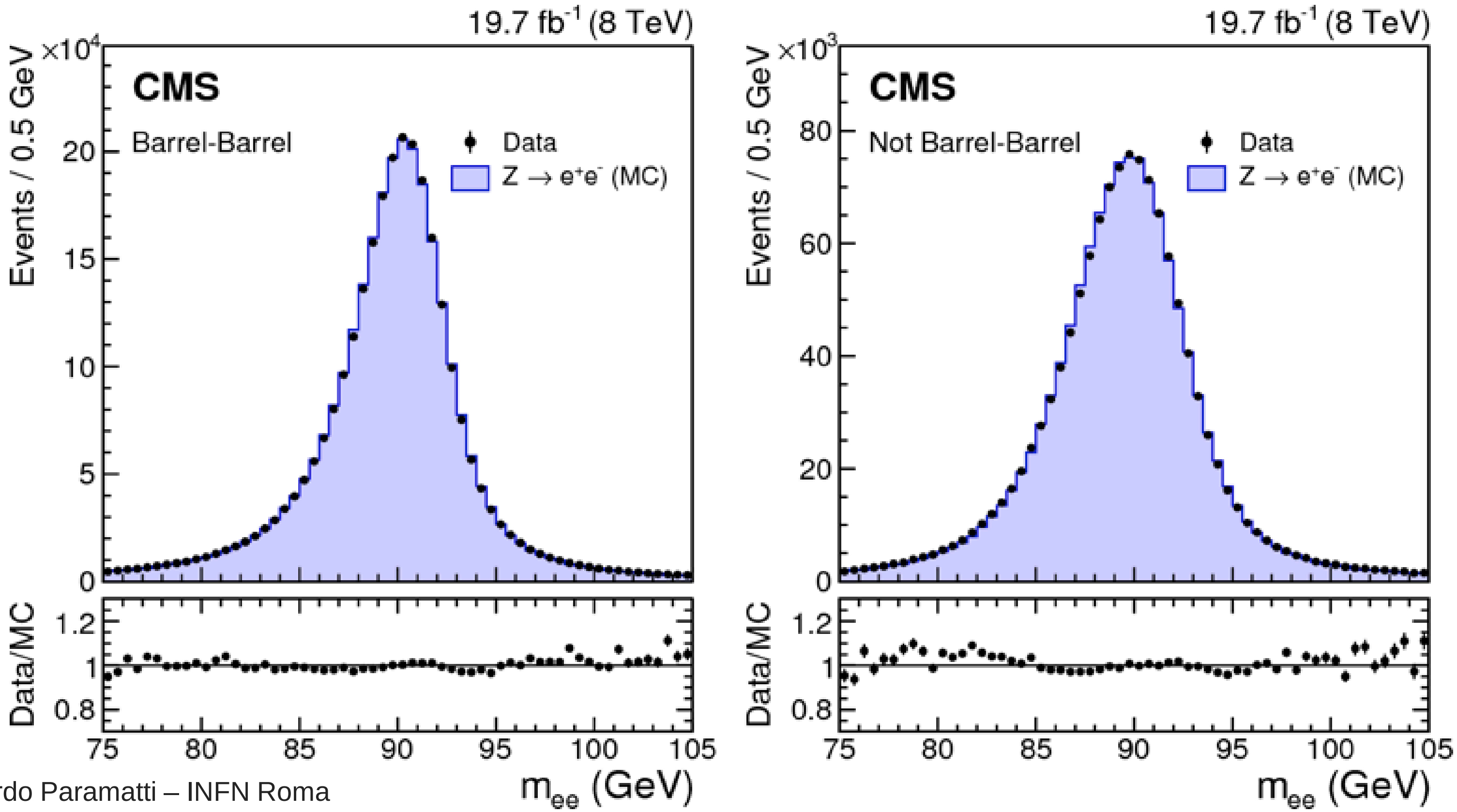

…in ATLAS life is complex as well…

LAr

cell energy

digital-to-analog converter on calibration board

ADC to DAC

optimal filter coefficients

$$E_{\text{cell}} = F_{\mu A \to \text{MeV}} \cdot F_{DAC \to \mu A} \cdot \frac{1}{\frac{M_{\text{phys}}}{M_{\text{cali}}}} \cdot R \left[\sum_{j=1}^{N_{\text{samples}}} a_j \left(s_j - p \right) \right]$$

ionization current to energy deposited; depends on sampling fraction

response of physics pulse vs. calibration pulse

pedestals

Reconstruction of the Liquid Argon cell energy in ATLAS

…in ATLAS life is complex as well…

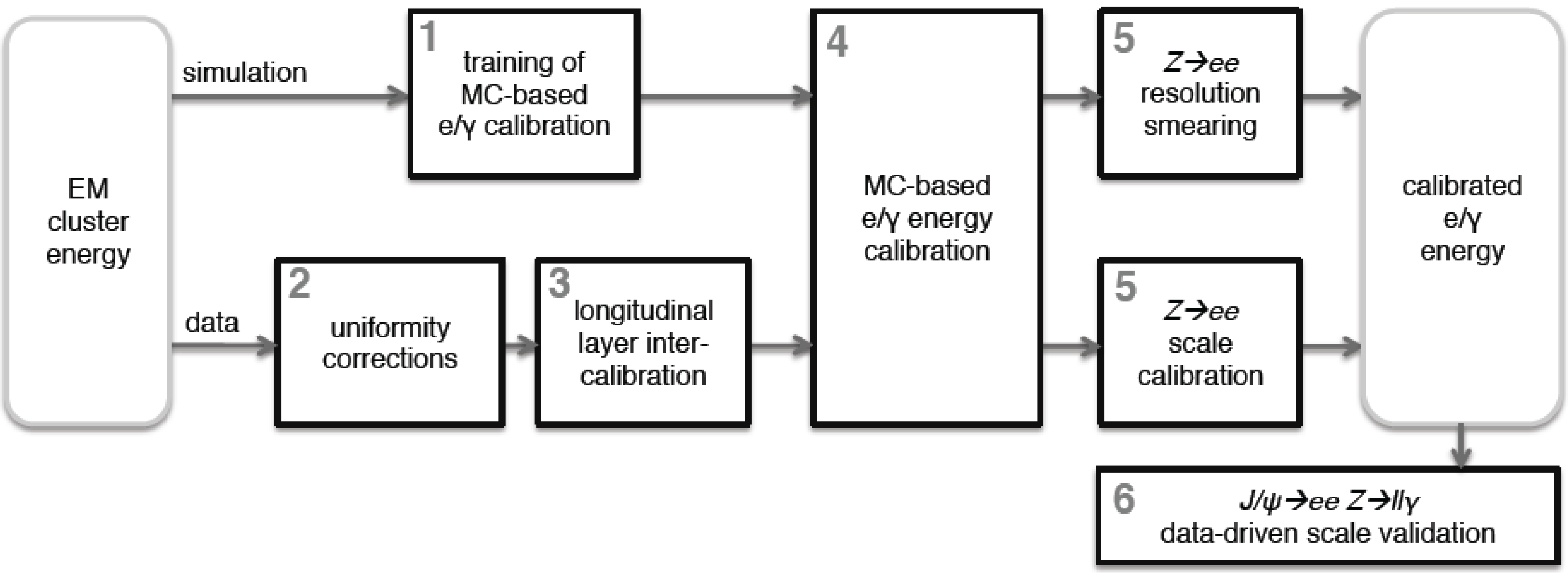

Schematic overview of the procedure used to calibrate the energy response of electrons and photons in ATLAS

…and material in front of calorimeter matters as well

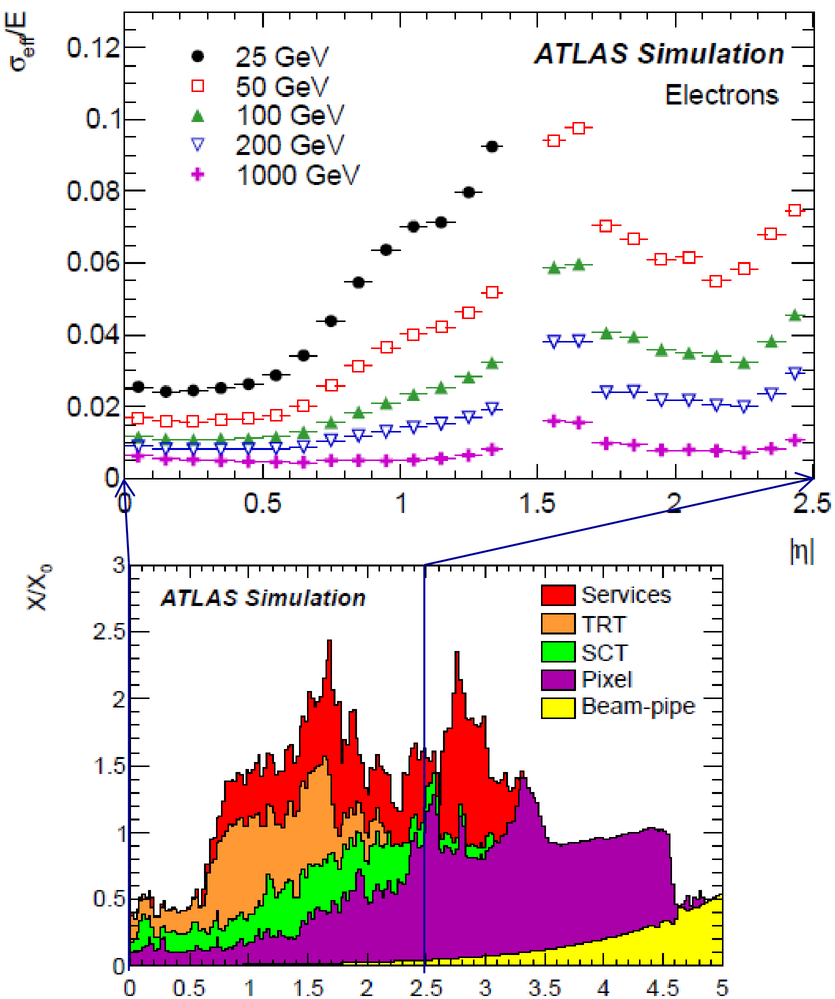

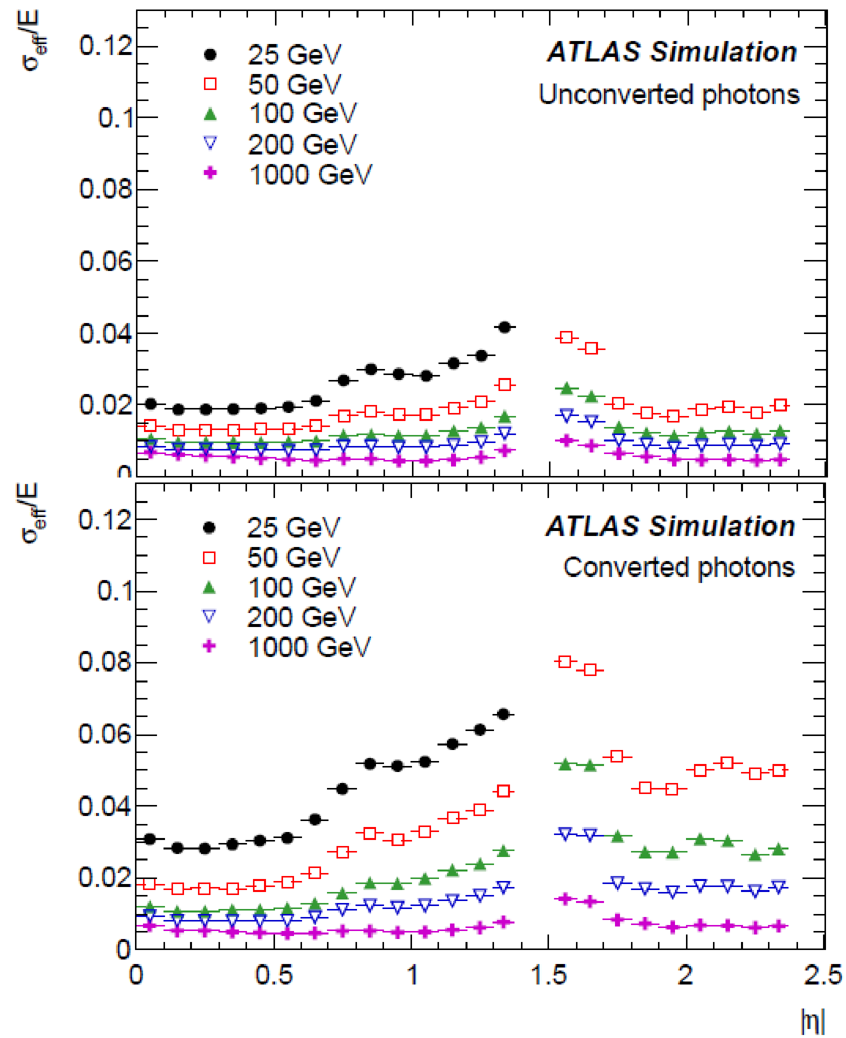

...still excellent (and similar to CMS) performance

- Fraction of working channels during LHC Run1: LAr 99.1%, Tile 99.6%
- Timing stability and resolution.

LAr Timing Stability vs. LHC Fill # in 2012

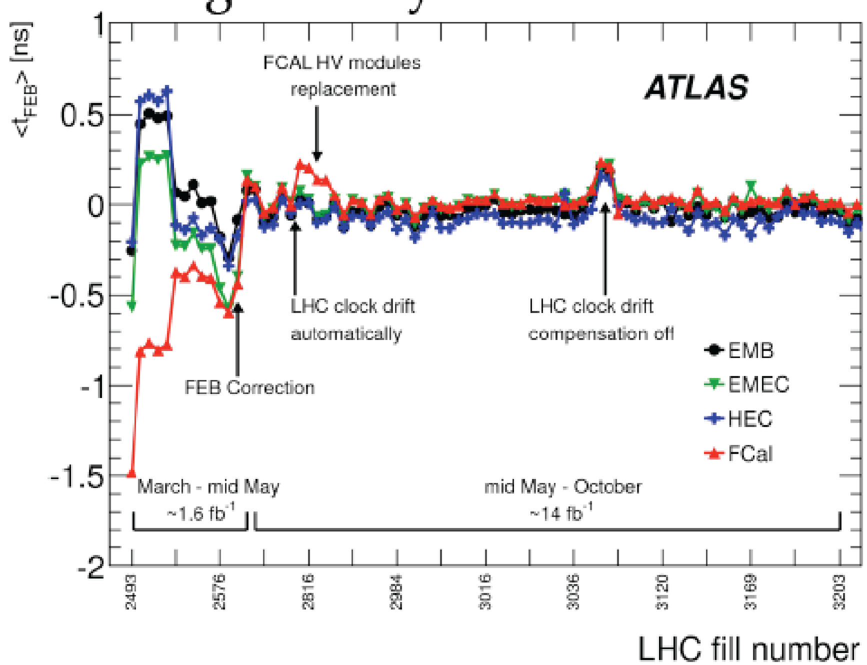

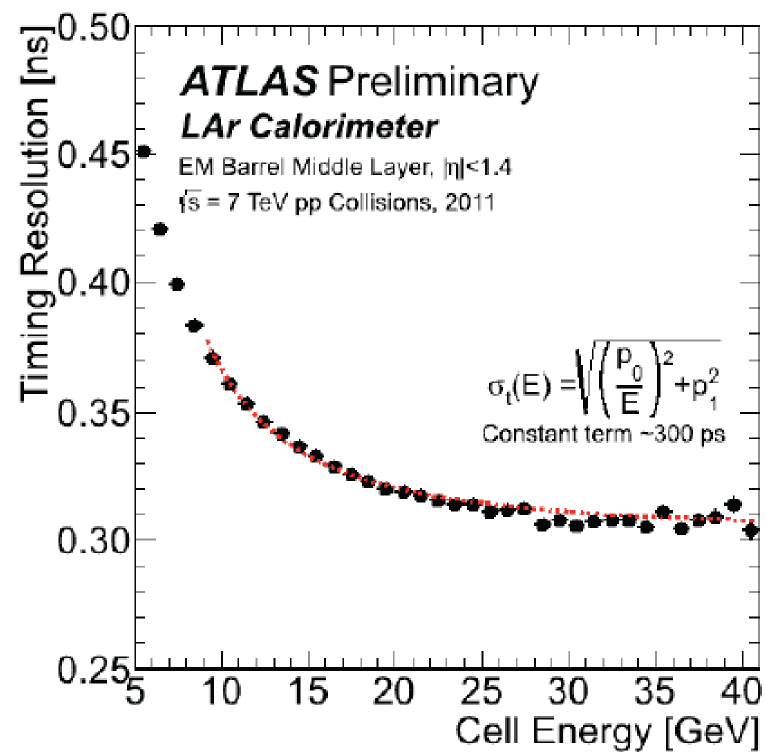

Energy response stability and electron reco efficiency

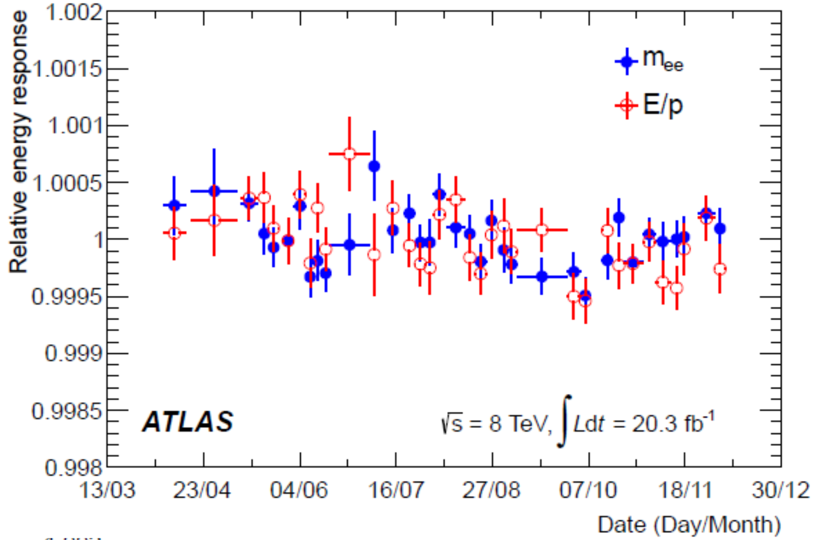

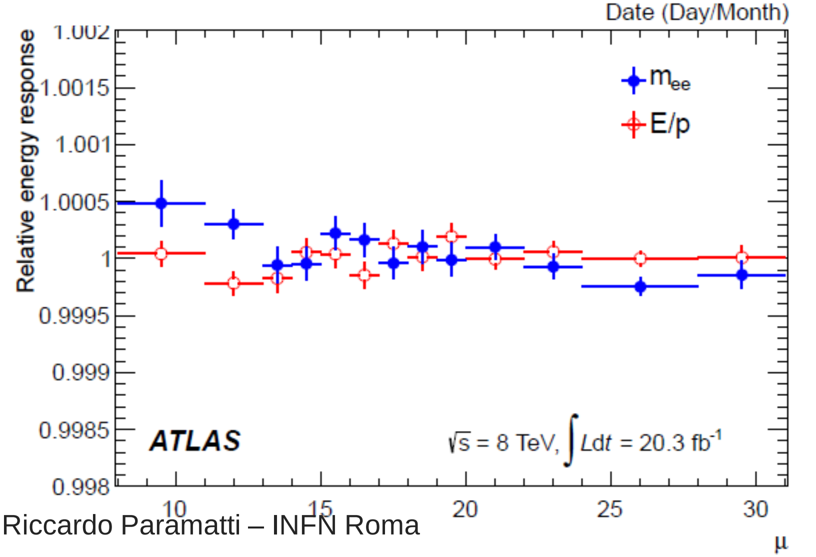

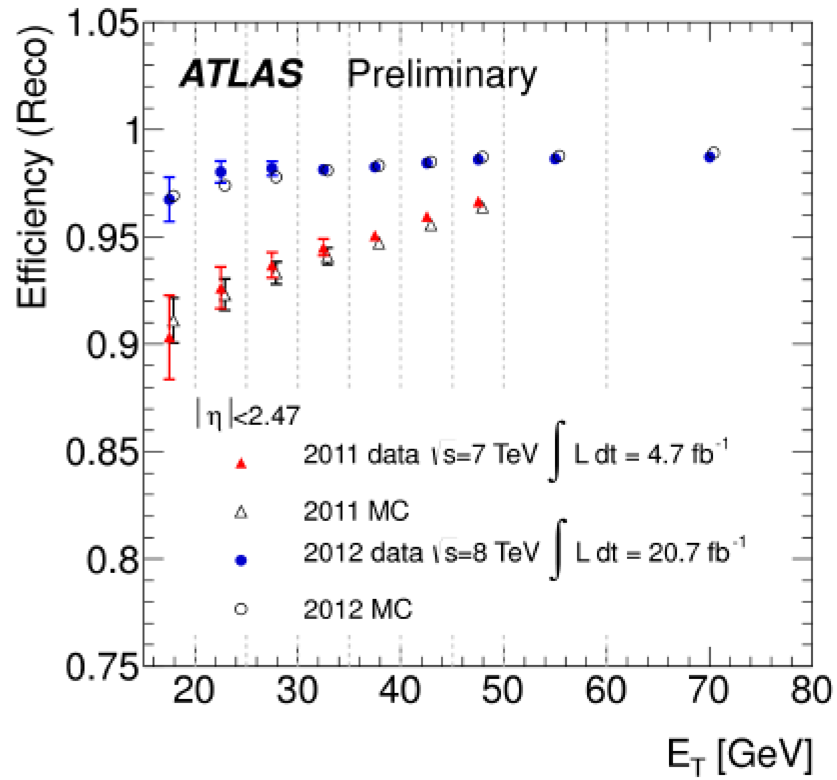

Energy scale and smearing

Energy scale ($E^{\mathrm{Data}} = E^{\mathrm{MC}} \times (1+\alpha)$)

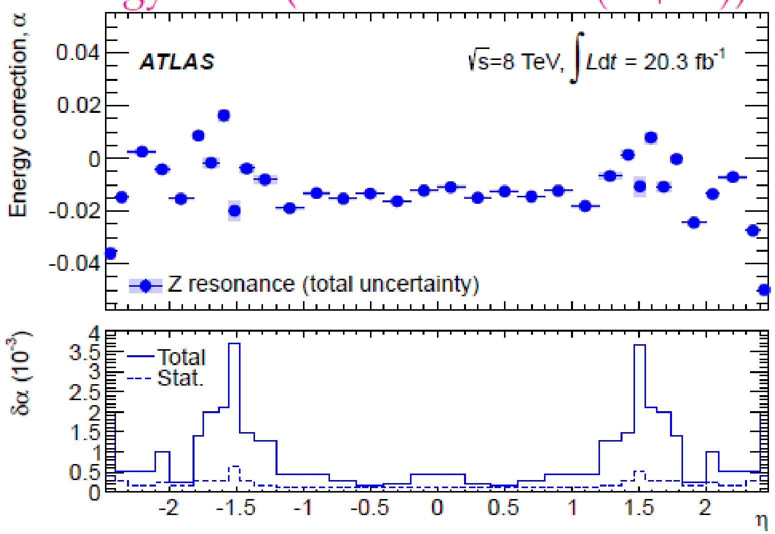

Effective constant term ($\sigma^{\mathrm{Data}} = \sigma^{\mathrm{MC}} \oplus c \times E$)

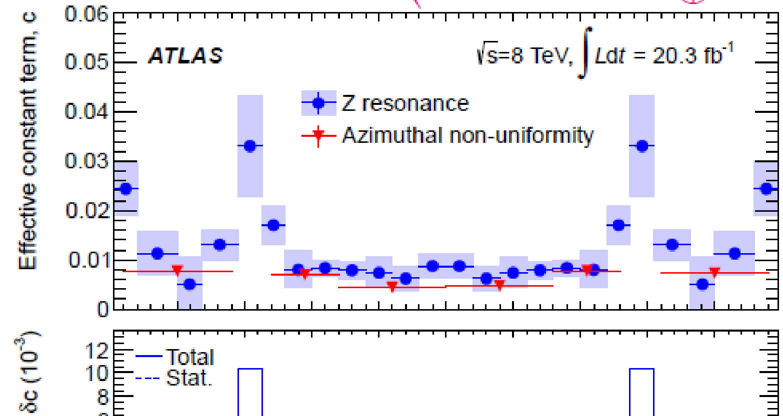

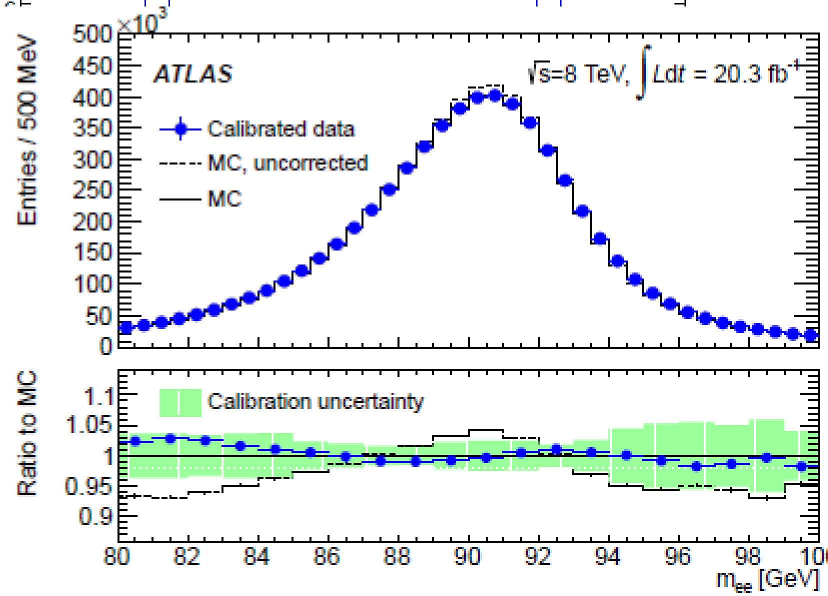

- Energy scale and energy smearing brings to a very good data-MC agreement.

Hadronic calorimeter performance

Jet and Missing Transverse Energy

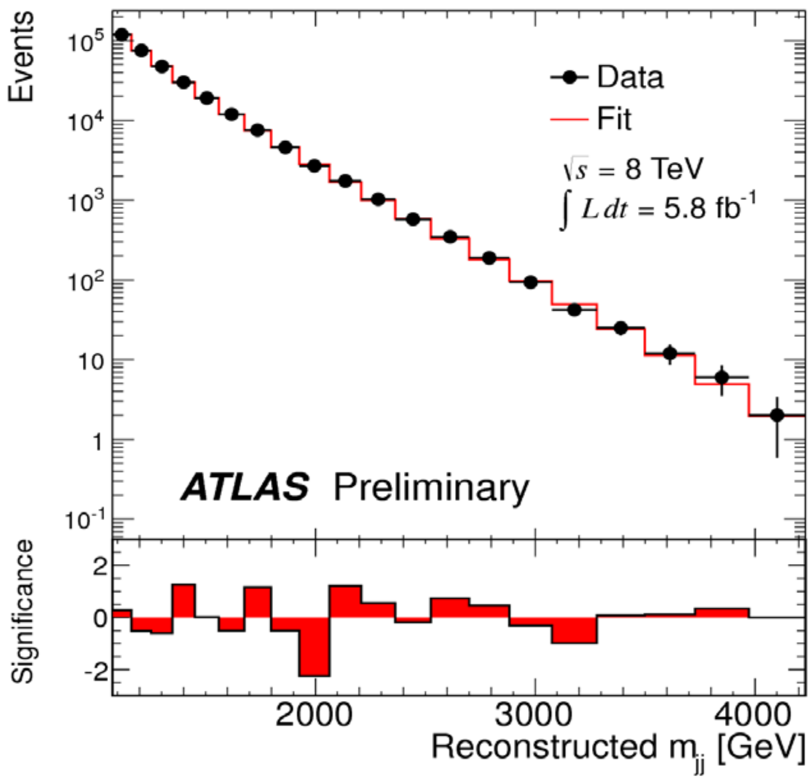

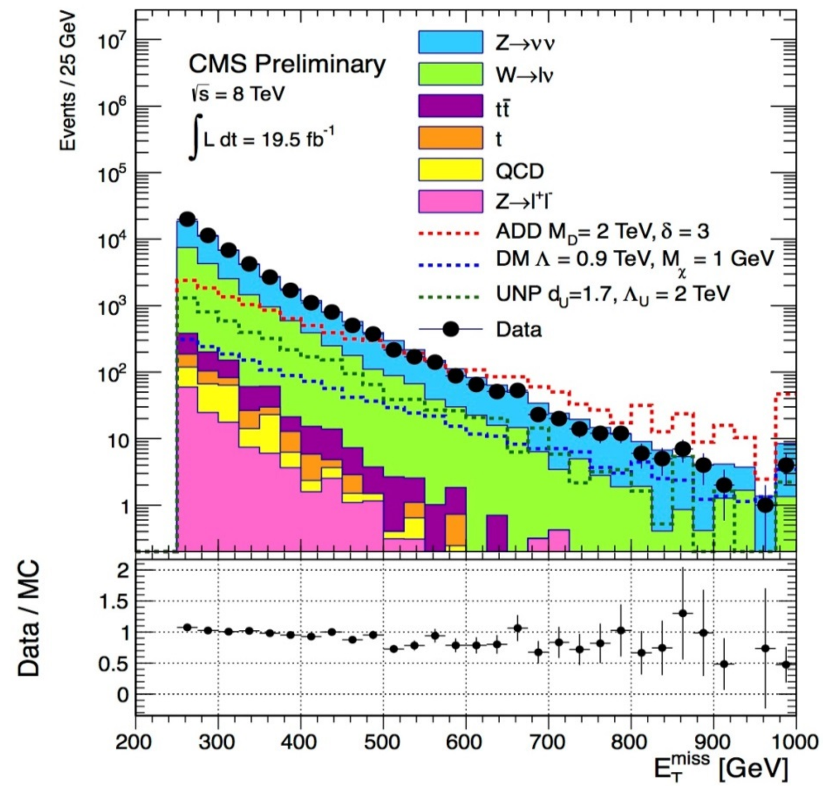

Crucial energy measurements in the quest for new physics!

ATLAS and CMS use different approaches:

- Calorimetric (ATLAS)
- Particle Flow (CMS)

Hadronic energy resolution

ATLAS test beam

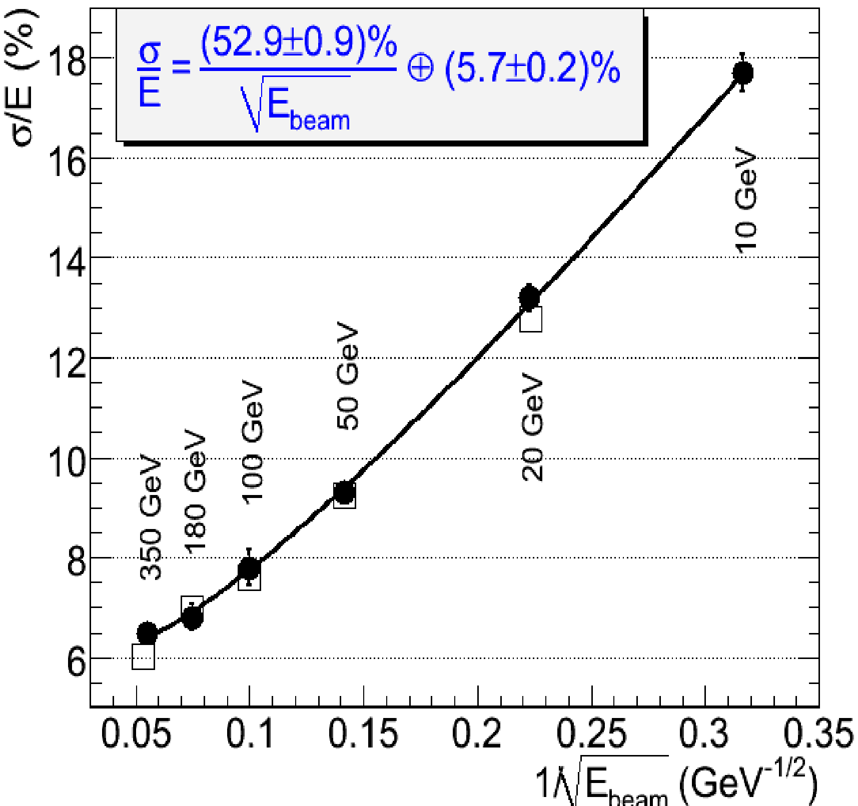

CMS test beam

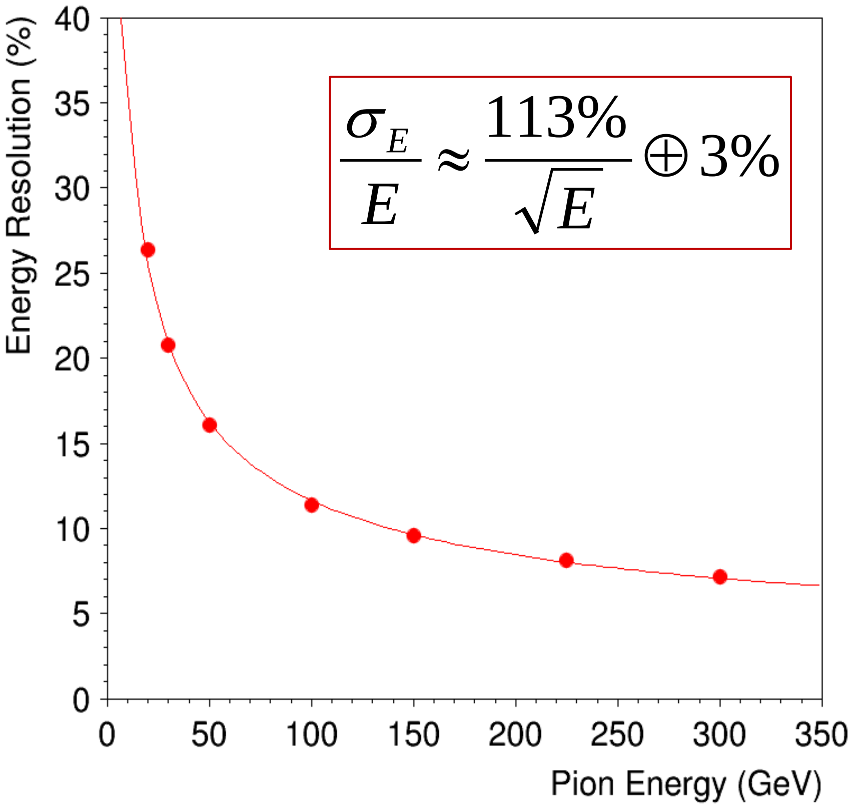

Jets from collisions

We are not going to measure single hadrons…

Types of jets:

- Parton level –quarks/gluons from initial collision
- Hadron level –fragmentation, decay, hadronization produce particles
- Experimental –what we see in the calorimeter, and how we interpret it

Goal: take detector information to reconstruct parton level physics.

Several jet reconstruction algorithms used at hadron colliders (not covered in this lecture).

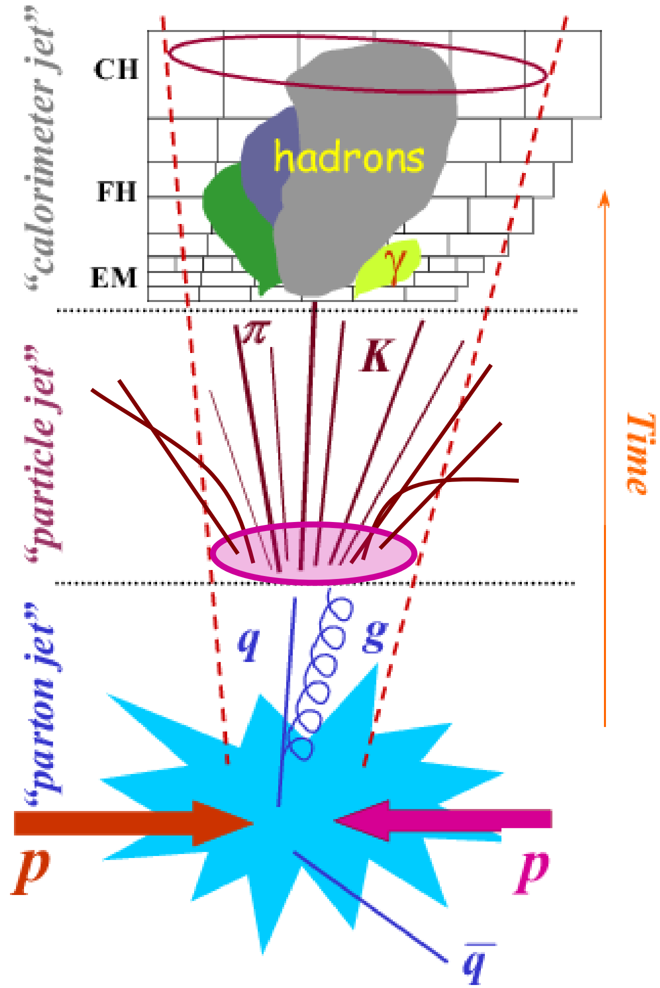

Use physics events to understand jet energy reconstruction: $\gamma/Z(\rightarrow ll)$ + jet, $W \rightarrow jj$, …

Particle ID in Calorimeters

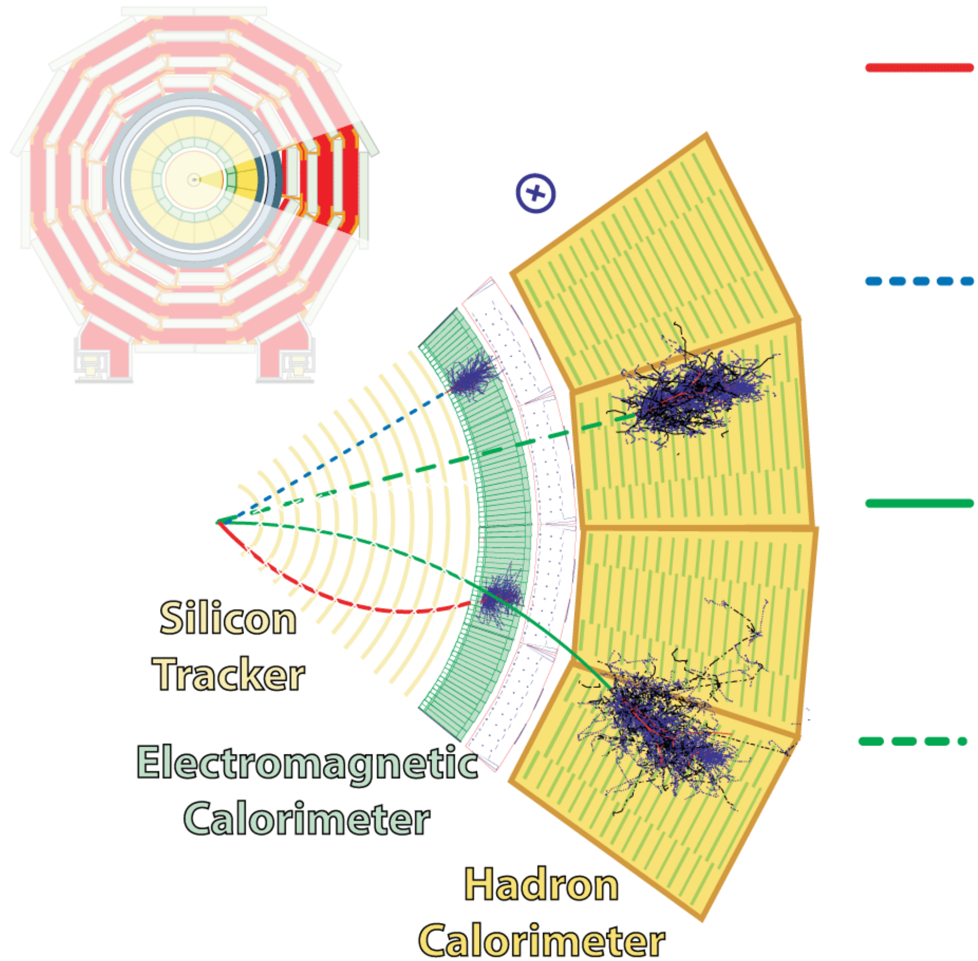

Electron

Curves in B field: R=P/0.3B
Signals in Tracker
Energy deposit in ECAL
No energy in HCAL

Photon

No curve in B field
No signals in Tracker
Energy deposit in ECAL
No energy in HCAL

Charged hadron (e.g. pion)

Curves in B field: R=P/0.3B
Signals in Tracker
Possible energy deposit in ECAL
Energy deposit in HCAL

Neutral hadron (e.g. neutron)

No curve in B field
No signals in Tracker
Possible energy deposit in ECAL
Energy deposit in HCAL

Particle Flow technique (in ALEPH, CMS,…, R&D)

Use the best system you have to measure particles in the event

Typical jet composition:
- charged hadrons (~ 60%)
- neutral hadrons (~ 10%)
- photons (~ 30%)

Cluster single particles in Jets

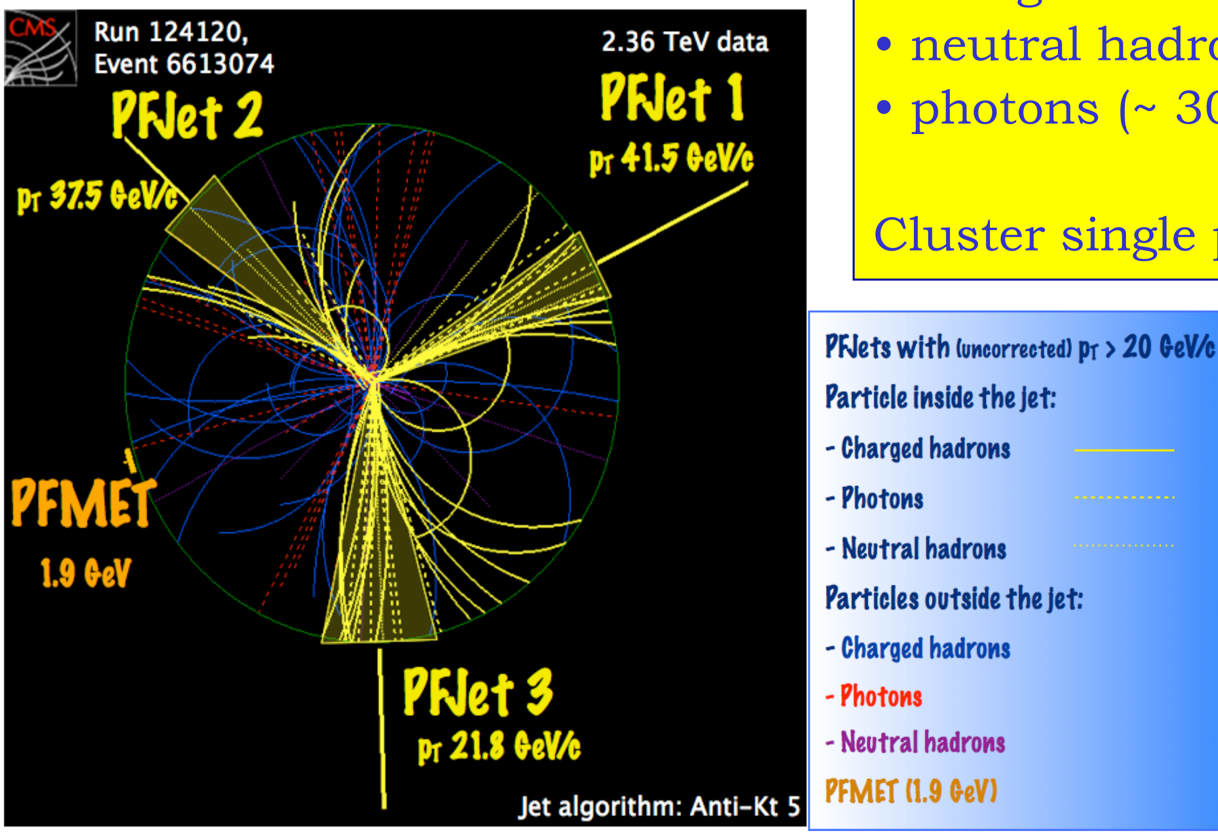

Multijet @ 2.36 TeV

CMS:
- high B
- excellent TK
- granular ECAL

Strong improvement in JET/MET resolution

Jet energy resolution

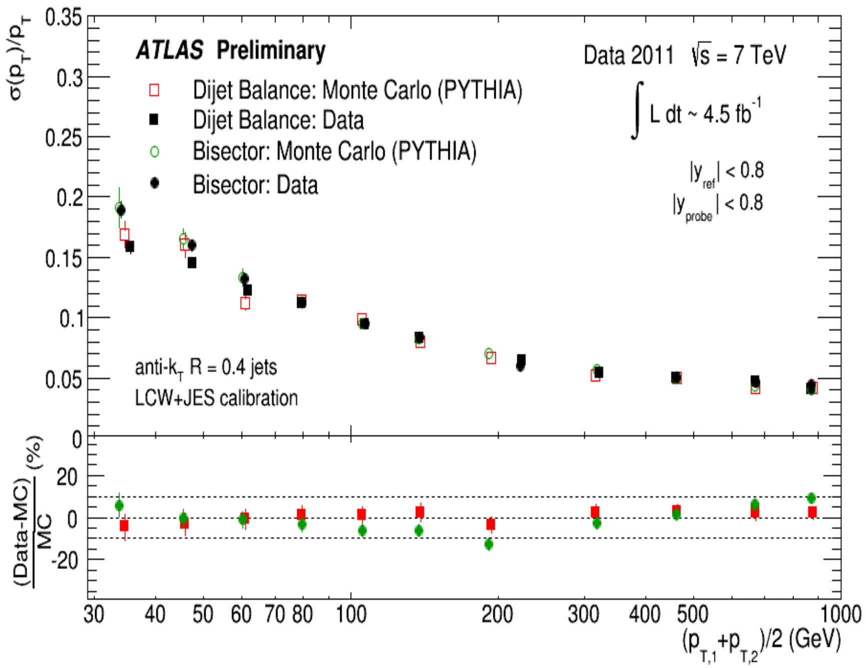

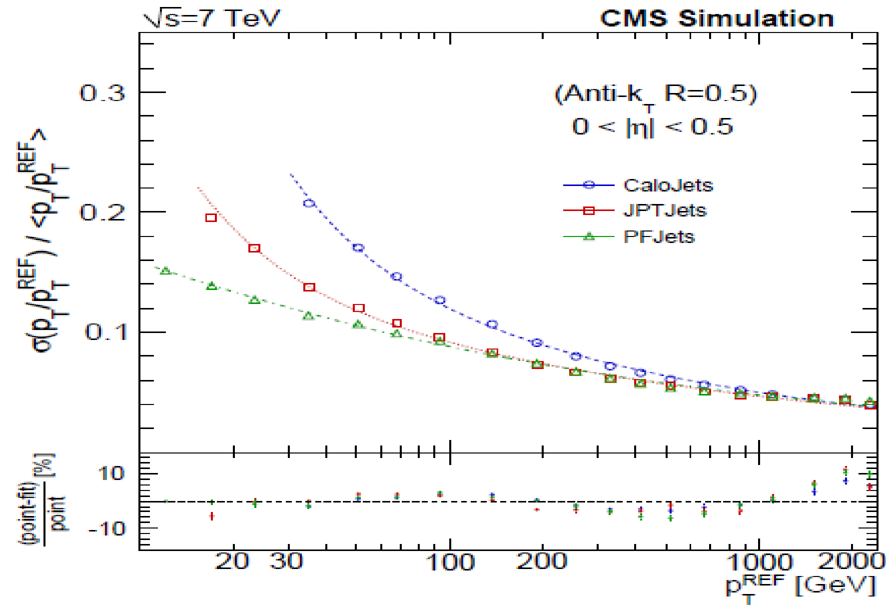

$\sigma(p_T)/p_T \sim 20\%$ @ $p_T = 30$ GeV
$\sigma(p_T)/p_T < 10\%$ $p_T > 100$ GeV

$\sigma(p_T)/p_T \sim 12\%$ @ $p_T = 30$ GeV
$\sigma(p_T)/p_T < 10\%$ $p_T > 100$ GeV

- Similar performance in the region relevant for new physics with CMS Particle Flow. Atlas is better comparing calorimetric resolution.
- CMS slightly better in the region of SM physics

Particle Flow vs Calorimetric Jets in CMS

Jet response: $(p_T^{rec} - p_T^{gen}) / p_T^{gen}$

Resolution for the calibrated MET for multijet events with two jets with p_T>25 GeV

~ 60% of Jet Energy measured with tracks: no invisible energy and no energy dependent f_{em}

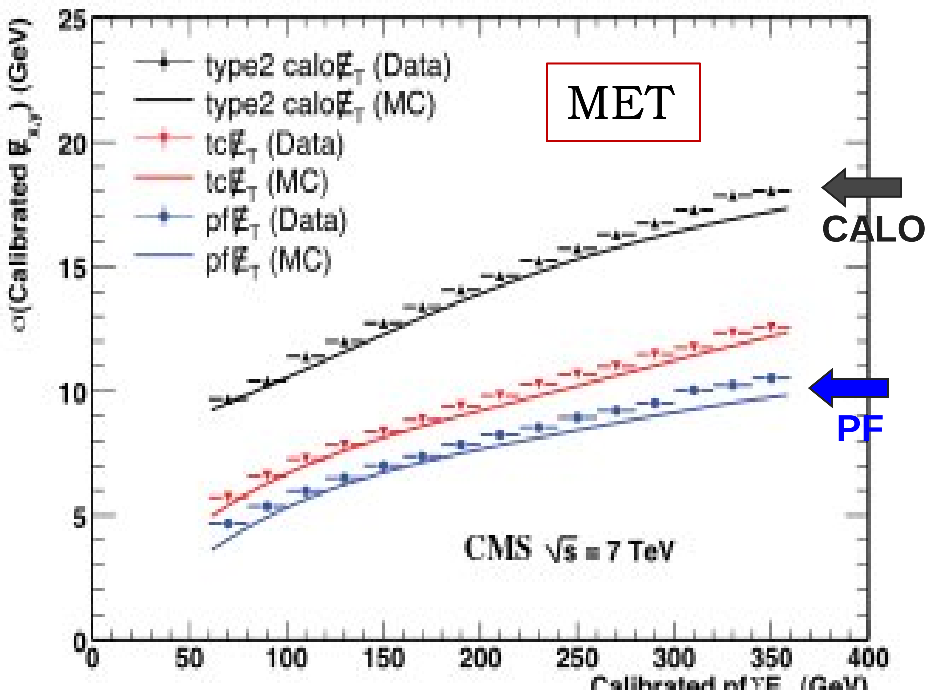

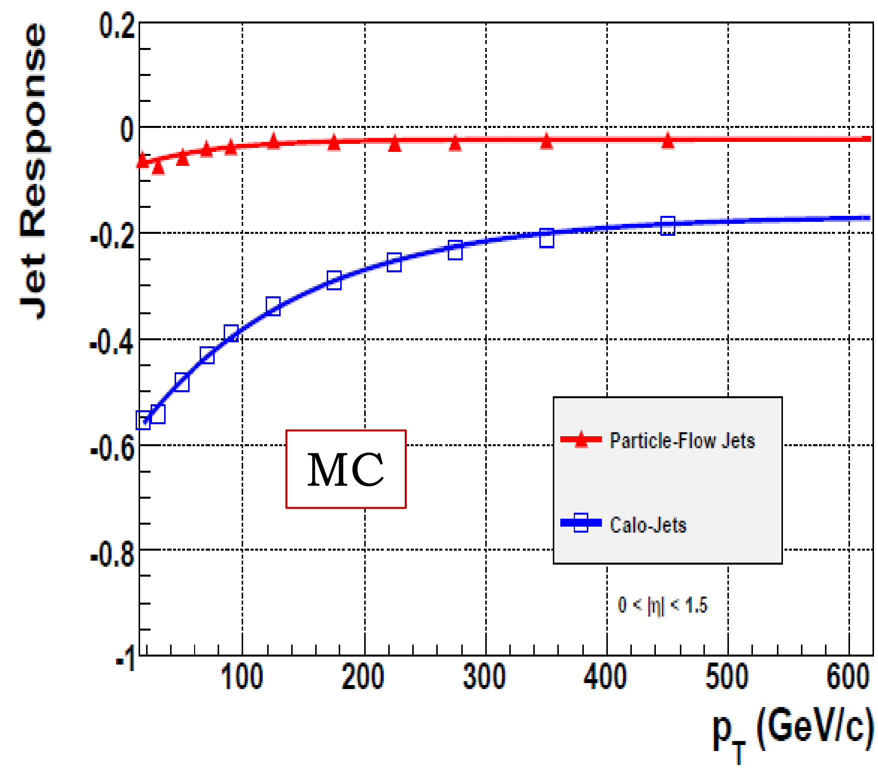

Missing transverse energy

$$\vec{E}_T^{\,miss} = -\sum_i \vec{E}_T^{\,i}$$

$$\not{E}_T = \left|\vec{E}_T^{\,miss}\right|$$

First step to measure MET: understand what is going on in your detector !

- Beam background, cosmics, various kind of noise some of which not really expected.
- Special filters developed to eliminate noise, which could otherwise affect MET performance

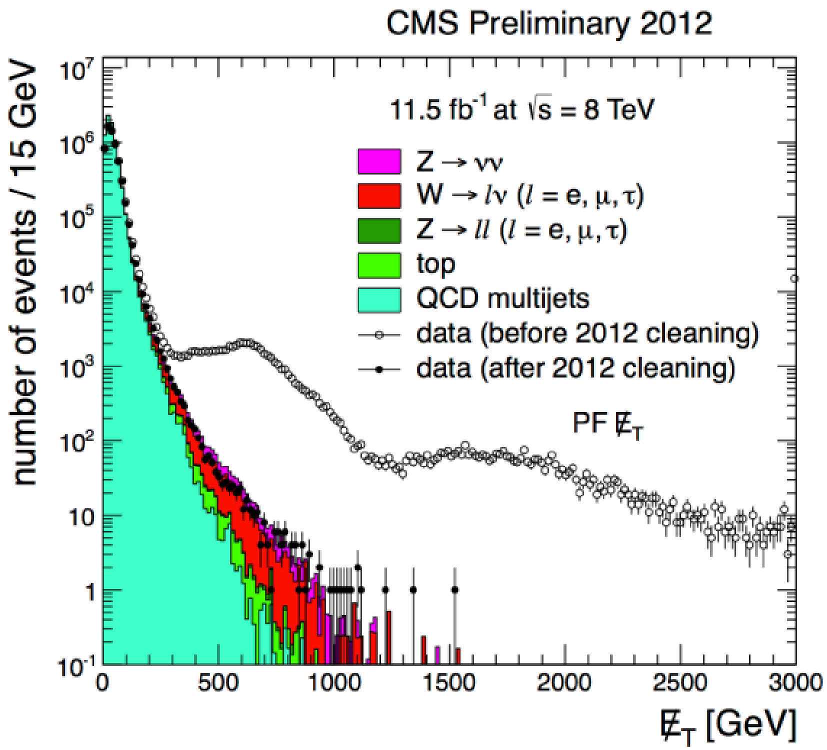

Distributions after detector cleaning, Including tails, very well reproduced by MC.

missing E_T resolution

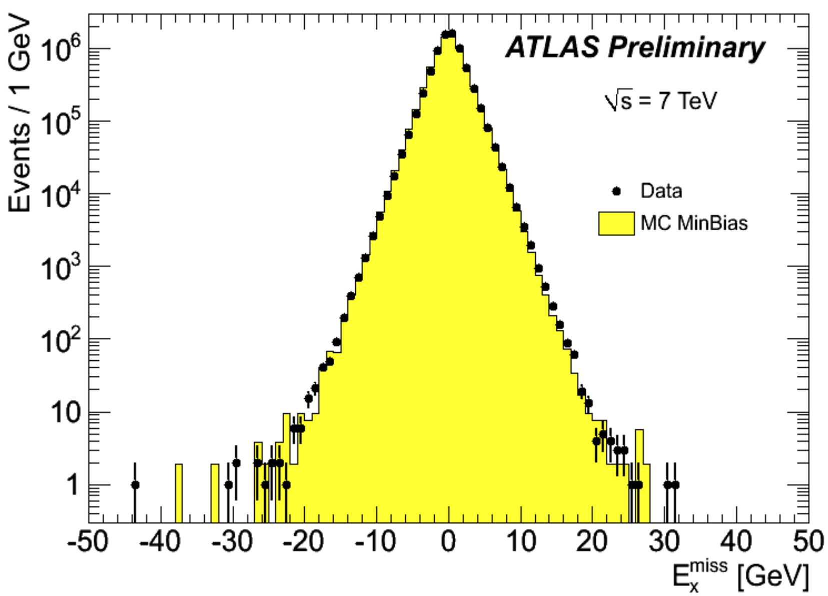

Atlas: ~37%$\sqrt{\Sigma E_T}$

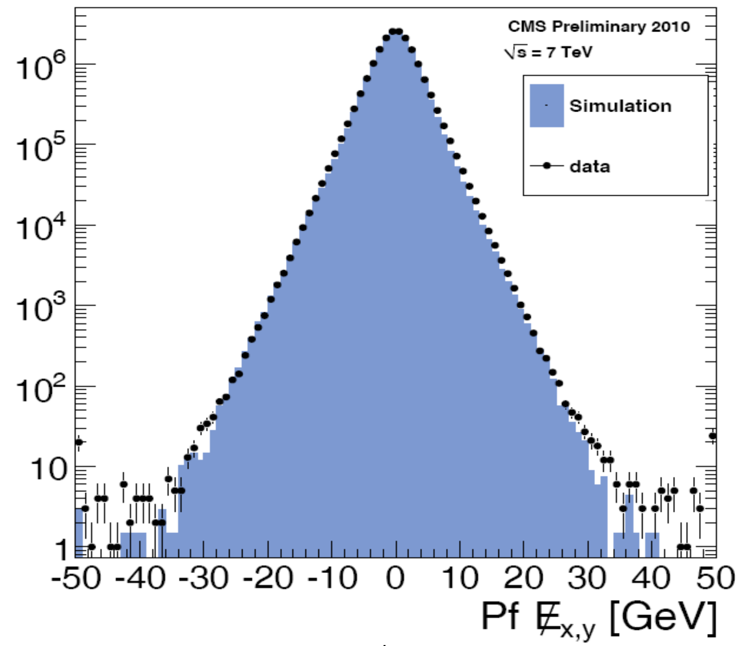

CMS: ~ 45%$\sqrt{\Sigma E_T}$

Again, thanks to the Particle Flow reconstruction, CMS recovers ATLAS performance on jets and MET and circumvents the non brilliant performance in hadron energy measurement.

Atlas and CMS calorimeters played a crucial role in the discovery of the Higgs Boson